Mussel Chemistry and Transcriptomic Response after a Minor Alaskan Oil Spill

Lizabeth Bowen[a*], William B. Driskell[b], James R. Payne[c], Austin Love[d], Shannon Waters[a], Eric Litman[e], Brenda Ballachey[f]

a: U.S. Geological Survey, Western Ecological Research Center, One Shields Avenue, Davis, CA 95616, USA; *lbowen@usgs.gov*; swaters@usgs.gov

b: Consultant, 6536 20th Avenue, NE, Seattle, WA 98115, USA; bdriskell@comcast.net

c: Payne Environmental Consultants, Inc., 1651 Linda Sue Lane, Encinitas, CA 92024, USA; jrpayne@sbcglobal.net

d: Prince William Sound Regional Citizens' Advisory Council, 130 S. Meals Suite 202, Valdez, AK 99686, USA; Austin.Love@pwrsrcac.org

e: NewFields Environmental Forensics Practice LLC, 300 Ledgewood Place, Suite 205, Mansfield, MA 02370, USA; elitman@newfields.com

f: U.S. Geological Survey (Emeritus), Alaska Science Center, 4120 University Drive, Anchorage, AK 99508, USA; beballachey@gmail.com

*Corresponding Author: Lizabeth Bowen lbowen@ucdavis.edu

September 22, 2021

Prince William Sound Regional Citizens' Advisory Council Contract numbers: 951.21.05 & 951.21.07

Contents

Abstract

A minor onshore oil spill (sump overflow) at the Valdez Marine Terminal (Port Valdez, Alaska) in April 2020, reached the shoreline and subsequently became a marine spill-of-opportunity from which to measure hydrocarbon concentrations and gene transcription in exposed intertidal mussels (*Mytilus trossulus*) along temporal (83 days) and spatial gradients. Mussel depuration rates showed half-lives for total polycyclic aromatic hydrocarbons (TPAH43) at 9.2 days, but individual analytes showed highly varied patterns (accumulation versus simple depletion) with depuration rates related to their partitioning coefficients (log K_{OW}). Petroleum biomarkers, with their high log K_{OW} and expected high lipid affinity, did not bioaccumulate. Transcription levels and hydrocarbon profiles and concentrations were compared with data from local and regional studies. Alaska North Slope crude-oil components in mussel tissues resulted in significant physiological responses that persisted with diminishing concentrations. These results suggest synergistic benefits to joint transcription and chemistry monitoring programs.

Graphical Abstract

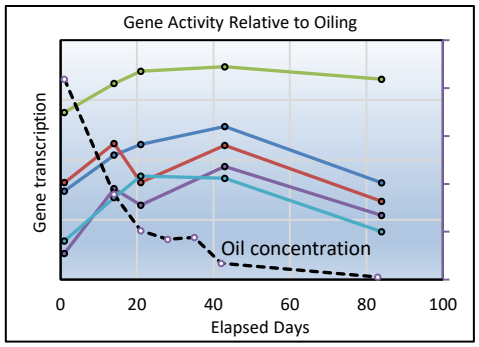

Keywords: gene transcription, PAH, petroleum biomarkers, detoxification, depuration, log K_{OW}, lipid affinity.

Funding Sources: This work was supported by the Prince William Sound Regional Citizens' Advisory Council under Contract Nos. 951.21.05 and 951.21.07.

1. Introduction

Historically, oil-spill monitoring in the marine environment has relied heavily on hydrocarbon identification and assessing tissue burdens as an indicator of a toxic insult, e.g., exceeding physiological threshold levels. From a chemistry perspective, crude oil is a complex mixture of tens of thousands of different components (McKenna et al., 2013) and evaluating the toxicity of newly identified oil hydrocarbons is an emerging science. Current assessment practices still emphasize polycyclic aromatic hydrocarbons (PAH) as the main concern in organismal toxicity (Sørhus et al., 2020), as will this study.

Exposure to PAH, even at low concentrations, can induce pathophysiological changes that may be subtle yet significant, and difficult to detect using classical diagnostic methods (Peterson et al., 2003; Hylland, 2006; Bodkin et al., 2014; Incardona et al., 2014). Perspectives on effective monitoring regimes are changing with continuing advances in biomolecular assessment techniques, including transcriptomics (Lowe et al., 2017). During gene transcription, information from a particular gene's DNA template is transcribed into messenger RNA (mRNA) and eventually translated into a functional protein. Changes in gene transcript levels can identify the organism's response to stressors, e.g., chronic or acute oiling. While the amount of mRNA transcribed from the gene is physiologically dictated by a number of intrinsic and extrinsic factors, the transcription response provides information about the organism's physiological changes and potentially deleterious effects (Snell et al., 2003; Lettieri, 2006). These early signs of altered gene transcription may be warning of broader ecosystem effects prior to visible manifestations in the organism or population (Farr and Dunn, 1999; McLoughlin et al., 2006; Poynton and Vulpe, 2009; Bowen et al., 2018). For acute events, transcription can serve as an indicator of recovery, i.e., return-to-normal, non-stressed transcription levels.

Filter-feeding mussels are excellent sentinels for the presence, bioavailability, exposure, and persistence of oil in the ecosystem (Livingstone et al., 2000; Bolognesi and Cirillo, 2014; Bowen et al., 2018). They are integral to the nearshore food web as a significant food source for both marine and terrestrial predators, and where abundant, are major structural components of the intertidal community. Mussel depuration rates are thus relevant to several spill recovery issues.

In some sense, accumulation and depuration of contaminants are mirror processes. Accumulation occurs through ingestion or absorption (e.g., finite oil droplets or dissolved components in siphon, mantle, or gill tissues) and inversely, depuration through gut elimination, diffusive desorption or metabolism, e.g., conversion through the aryl-hydrocarbon-receptor (AHR) pathway (Zanette et al., 2013). Higher ambient oil

concentrations and longer duration chronic exposures imply increased accumulation and longer depuration times. These factors, plus the variety of hydrocarbons with their individual water-versus-lipid solubility, and even the prior health of the mussels, dictate that each spill event will be unique in degree of impacts and achieving recovery. Here, mussel transcription responses are documented following an acute oiling event and subsequent diminishing chronic exposure.

In April 2020, a minor oil spill occurred at Alyeska's Valdez Marine Terminal, Prince William Sound, Alaska, whereby an estimated 1,400 gallons (34 bbls) of Alaska North Slope (ANS) crude oil overflowed from a sump well, traversed undetected as a subsurface downslope plume (below ground and snow cover), and subsequently emerged at the nearby shoreline, creating slicks and necessitating a full-scale marine response. Recognizing a spill-of-opportunity, the Prince William Sound Regional Citizens' Advisory Council initiated a special project to measure petroleum hydrocarbons and gene transcription in intertidal mussels (*Mytilus trossulus*) exposed to the spilled oil on both spatial and temporal scales. The primary goals were to determine oil concentrations and depuration rates for the impacted mussels and measure gene transcription relative to the depuration process. Mussels were included from the oil-monitoring project from the Council's annual Long Term Environmental Monitoring Program (LTEMP) collected at 52 days post-spill from nearby sites (~1 km) bracketing the spill origin. The previous year's LTEMP collections provided recovery endpoints and comparisons to historic background data (Payne and Driskell, 2020).

2. Materials and Methods

2.1. Sampling

The Valdez Marine Terminal (Prince William Sound, Alaska) is the terminus of the Trans-Alaska Pipeline, bringing Alaska North Slope (ANS) crude oil to load tankers in Port Valdez for shipment to west coast refineries. Annual sampling for the LTEMP monitoring program occurs in June/July adjacent to the shipping berths at Saw Island (AMT) and Jackson Point (JAP) (Fig. 1). The spill occurred between these two sites and comprised primarily ANS crude oil plus terminal runoff.

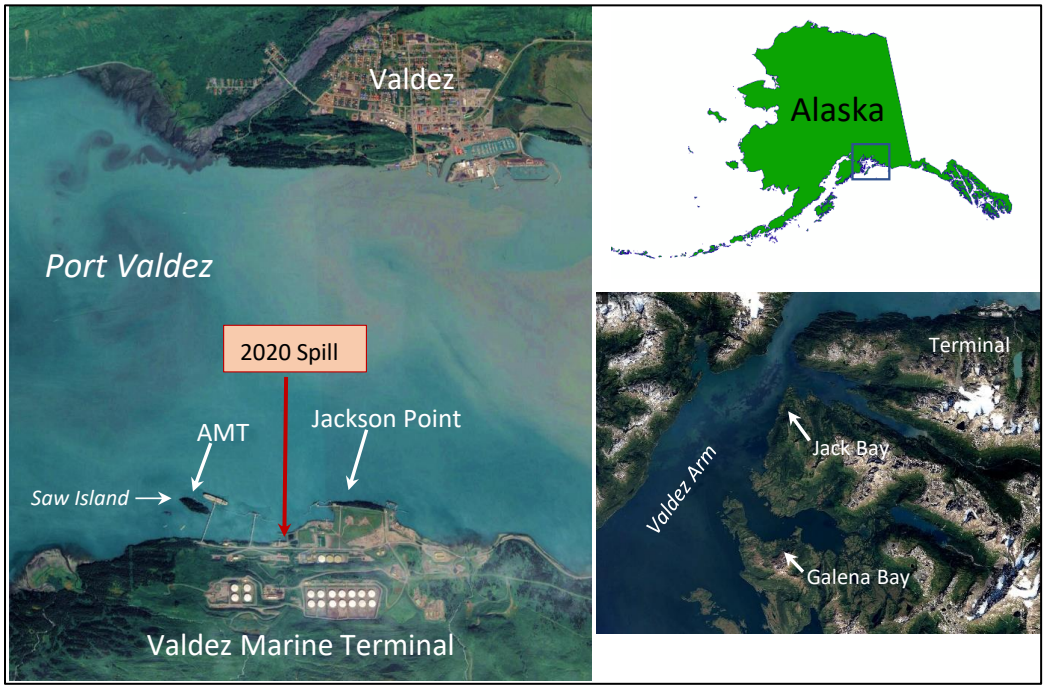

Fig. 1. *Overview of Port Valdez (inset A) showing the April 12, 2020 intertidal spill location at the Valdez Marine Terminal. Mussels were sampled at the Spill Site ("Hot Zone"), Jackson Point (JAP), and Saw Island (AMT). Regional background samples were collected at Jack Bay and Galena Bay (inset B) in June 2020.*

As the spill reached the shoreline, the plume was containment boomed and partially removed (Fig. 2), but sheening from lingering oil still leaking from the sump and the saturated sediments continued through the study. A gradient of shoreline sampling sites was established (Fig. 1), including the traditional LTEMP stations, and sampling begun 19 days after the initial spill event. Mussels for chemistry and transcription analyses were collected concurrently throughout the time series but to manage analytic budgets, not all were processed (Table 1). Each transcription replicate analysis represents an individual mussel; chemistry replicates were composites. As transcription results came back,

decisions were made to analyze respective chemistry replicates. Non-exposed mussels were collected for controls from remote locations, Jack Bay and Galena Bay, within the Port Valdez fjord (Fig. 1).

Fig. 2. *Spill site and visible oil and sheen observed inside the containment booms at Valdez Terminal in April 2020. Photos courtesy of Alyeska Pipeline.*

Table 1. *Samples included in chemistry and transcription analyses. PV19 is average of samples collected in Port Valdez in 2019; PV20 in 2020.*

Location	Date*	Elapsed days of study	Chemistry replicates	Transcription replicates
Spill site	4/30/2020	1	3	10
	5/13/2020	14	3	6
	5/20/2020	21	3	7
	5/27/2020	28	2	
	6/3/2020	35	2	
	6/11/2020	43	3	6
	7/22/2020	83	2	5
PV19 (avg)	6/15/2019 (LTEMP)	-361	6 at 2 sites	20 at 2 sites**
PV20 (avg)	6/9-6/11/20 (LTEMP)	41-43	6 at 2 sites; 1 at 2 sites	40 at 4 sites**

*Initial spill event (intertidal detection) was 12 Apr 2020.

** In 2019, mussels were sampled at Jackson Point and Saw Island. In 2020, in addition to samples from the Spill Site, mussels were sampled at Jackson Point, Saw Island, Jack Bay, and Galena Bay to obtain regional background values.

2.2. Chemistry

Collection and analytical methods are generally patterned after the NOAA Mussel Watch Program (Payne et al., 2008; Apeti et al., 2012; Payne et al., 2021). Briefly, three replicates of 30 mussels each are collected by hand at each site and immediately frozen for transport and archival before whole-body tissue compositing, homogenization, and extraction. Analyses were provided by Alpha Analytical Laboratory (Mansfield, MA) under the guidance of NewFields Environmental Forensics Practice LLC (Rockland, MA).

Standard forensic oil-hydrocarbon data are reported: polycyclic aromatic hydrocarbons

(PAH), saturated hydrocarbons (SHC), and sterane/triterpane petroleum biomarkers (S/T). Complete lists of PAH, SHC, and S/T analytes are presented in Appendix 2 along with the analyte abbreviations used throughout this paper.

The PAH, alkylated PAH, and S/T are analyzed as semi-volatile compounds using selected-ion-monitoring gas chromatography/mass spectrometry (SIM GC/MS) via a modified Environmental Protection Agency (EPA) Method 8270 aka 8270M (Stout and Wang, 2016). This analysis provides the concentration of approximately 80 PAH, alkylated PAH homologues, individual PAH isomers, and sulfur-containing aromatics, plus approximately 50 petroleum biomarkers including tricyclic and pentacyclic triterpanes, regular and rearranged steranes, and triaromatic and monoaromatic steroids. For SHC, a high-resolution gas chromatography/flame ionization detector (GC/FID) profile using modified EPA Method 8015B reports total extractable materials (TEM; C9-C44), n-alkanes (C9-C40) and selected (C15-C20) acyclic isoprenoids (e.g., pristane and phytane). Histogram bar plots of PAH, SHC, and S/T are examined against oil standards or method detection limits (MDL). Further details are provided in Appendix 2; results in Appendices 3 and 4.

2.3. Gene transcription

Collection and analytical methods are fully described in Appendix 1 and are generally patterned after standard sampling protocols (Bowen et al., 2018; Counihan et al., 2019). Briefly, mussels were collected by hand at each site and adductor muscles immediately excised and placed into RNAlater®. Samples were frozen and stored at -80oC until processing. Tissues were subsequently homogenized, RNA extracted, cDNA synthesized, and quantitative PCR performed according to standard protocols. All laboratory analyses follow MIQE guidelines (Bustin et al., 2009).

3. Results

3.1. Chemistry

Oil sourcing and weathering in the Alaskan environment have been well documented in the decades since the 1989 Exxon Valdez spill. For this study, the focus was not on the levels of oiling in the environment nor forensic source identification but rather on the component-specific recovery process (depuration) in mussel tissues and its relationship to gene transcription.

Both chemistry and spill-response observations establish that this spill was not a single exposure event. The mussels initially were acutely oiled by the emerging land plume (reported April 12; source mitigated April 13). Subsequently, the subsurface plume continued to sheen in diminishing amounts through the spring and summer, persisting after the project's last sampling in late July (light sheening confirmed in SCAT reports; pers comm, T. Larson, Alaska Department of Environmental Conservation). The containment booms stayed in place until October 2020.

3.1.1. Profiles

Three major oil fractions, PAH, SHC, and S/T, are used in this study to characterize spilled oil and accumulated residues in the tissues of exposed organisms (Fig. 3). Appendix 3 is a compendium of all profiles from mussel samples discussed in this study. Appendix 4 presents selected text-cited figures arranged and discussed to illustrate a particular time-series trend or spatial finding.

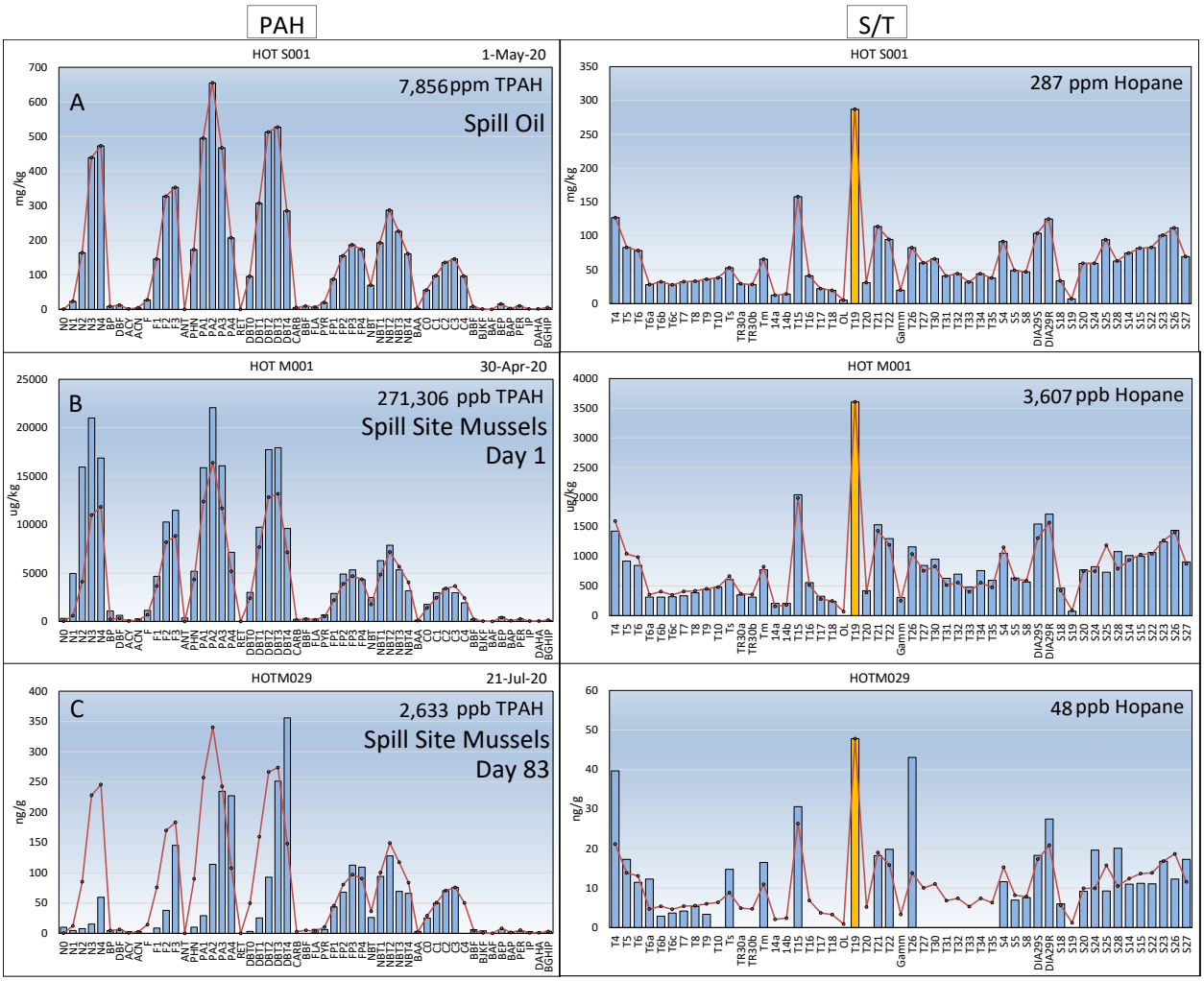

Fig. 3. *Profile plots of the PAH and petroleum biomarker (S/T) fractions of the spilled oil (A) and intertidal mussels from the Spill Site on study Days 1 (B) and 83 (C). The red line overlay denotes the Day 1 oil profile rescaled to the mussel sample's C2-chrysene for PAH and hopane for biomarkers. Weathering depletions are the empty spaces beneath the line. SHC are shown in Appendices 3 and 4.*

To facilitate comparing the spill-oil profile to those in tissues (Fig. 3), the concentration scales are plotted differently with the oil in parts per million (ppm) and the tissues in parts per billion (ppb). There is remarkable fidelity between the spilled-oil and the exposed mussel profiles although the PAH in mussels appears slightly fresher (i.e., the slight excess of lower-molecular-weight PAH above the red-lined, source-oil profile normalized to C-2 chrysene). This may reflect the mussels' earlier exposure to the fresher spilled oil, before the study's initial source sample (project Day 1) was collected from the shoreline 18 days after the spill began (see Fig. A4-3). By Day 83, however, the lighter-molecular-weight C1-C3 substituted PAH homologues are mostly diminished from the naphthalenes (N), fluorenes (F), phenanthrenes/anthracenes (P/A), and dibenzothiophenes (DBT). Note that later

weathering depletions appear as empty space beneath the red lines in the time-series profiles (Fig. 3).

These missing PAH constituents are more volatile and have greater water solubility compared to the higher-molecular-weight fluoranthene/pyrenes (FP), naphthobenzothiophenes (NBT), and chrysenes (C). As such, they are subject to natural (abiotic) weathering loss in a surface slick (particularly thin films and sheens), and theoretically, with higher water-solubility, they may exhibit enhanced depuration from an exposed organism. The sum effect of these component-specific removal mechanisms, continued weathering, and plume mitigation, albeit with persisting re-exposure, was that overall concentrations, total PAH (TPAH43), total SHC and hopane all diminished by several orders-of-magnitude over the 83-day project (Fig. 3 and Appendix 4). Profiles from adjacent LTEMP sites on Day 1 (Fig. A4-4) show dramatically reduced oiling compared to the spill site, demonstrating the effectiveness of the containment booming practices (Fig. 2).

Background (pre-spill) mussel samples were not available from the spill site, but LTEMP samples collected the previous year from Jackson Point (Fig. 1) showed ultra-trace background concentrations (Fig. A4-5). By Day 42-43, sixteen-fold differences in TPAH43 concentrations and twenty-five-fold differences in hopane were noted between spill site mussels and LTEMP stations (Fig. A4-6). Post-spill (Day 83) Jackson Point samples still contained minor amounts of heavily weathered, residual oil. Background PAH, SHC, and S/T profiles from control stations at Jack Bay and Galena Bay were essentially clean (Fig. A4-7), dominated by typical background traces of combustion-product PAHs and biogenic isoprenoids and n-alkanes (NRC, 1985). Hopane was not detected, and there was no evidence of petroleum hydrocarbon contamination at these remote sites.

Time-series plots of PAH, SHC, and S/T in mussels from the spill site (Fig. A4-8) show monotonic declines in lower-molecular-weight PAH components and elimination of the fence-post pattern of odd- and even-carbon number, petroleum-derived n-alkanes from n-C9 through n-C40 in the fresher oil, while biogenic isoprenoids (1380, 1470, and pristane) become more dominant with time (NRC, 1985). Residual traces of phytane and n-C22 to n-C40 alkanes in the Day 21 to 83 samples suggest continued exposure to heavily weathered oil sheens still present within the boom enclosures.

3.1.2. Depuration

The biomarker hopane, 17β(H),21β(H)-hopane (abbreviated as T19 in plots), is considered to be non-water soluble and mostly non-biodegradable and thus is among the best conserved of the petroleum components. Its non-biodegradable nature and the declining logarithmic shape of its depuration curve (Fig. 4 left panel) implies that simple elimination (gut-purging) dominates versus a mix of elimination, metabolic processing and/or

weathering. For the latter processes, the depuration curve would be expected to flatten or increase (bioaccumulate). A similar assessment was made for the 43-analyte PAH sum (TPAH43) (Fig. 4 right panel). Note that the TPAH43 index combines a wide range of solubilities with octanol/water partitioning coefficients ranging from 3-7 (log K_{OW}), which implies that each analyte is endowed with unique diffusive-desorption and gut-elimination rates. The resulting TPAH43 depuration curve represents a composite of those effects. Both hopane and TPAH43 depletions closely fit logarithmic-regression models (R2=0.96 for each). From these models, the half-life for hopane was calculated as 8.4 days while TPAH43 was 9.2 days, remarkably close values considering that certain members in the TPAH suite can bioaccumulate.

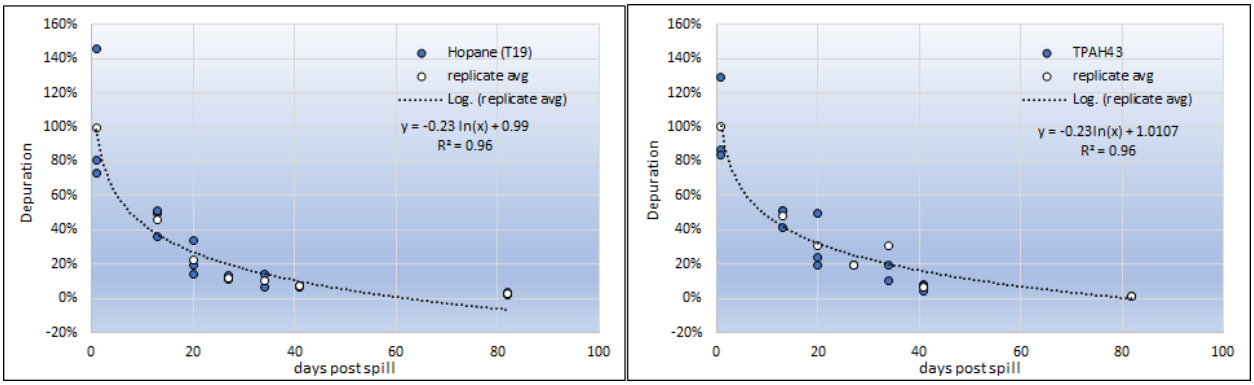

Fig. 4. *Depletion plots of hopane and PAH composite, TPAH43, in whole mussel tissues from the spill site. Both show simple depletion without bioaccumulation. Half-lives are 8.4 and 9.2 days, respectively. Solid dots are single replicates; white dots are averages.*

A few PAH examples of forensic interest show their varied rates of depletion (Fig. 5). In this study, most of the individual PAH present as various rates of simple depletion, by either log or exponential decay, and without accumulation, i.e., no initially increasing trends. However, there were exceptions. Higher-molecular-weight and higher-log-KOW PAH showed either accumulation or a more complex pattern (Fig. A5-1). As discussed below and in Appendix 5, there appears to be a transition from simple depletion mode into accumulation or mixed response modes for compounds with log K_{OW} > ~ 6.3.

In contrast, petroleum biomarkers plotted relative to hopane showed mostly flat lines with little depletion (Fig. 6). This suggests that similar to hopane (Fig. 4), the petroleum biomarkers in mussels undergo a simple depletion process (gut purging) without bioaccumulation. Depletion curves for all PAH are presented in the Appendix 5.

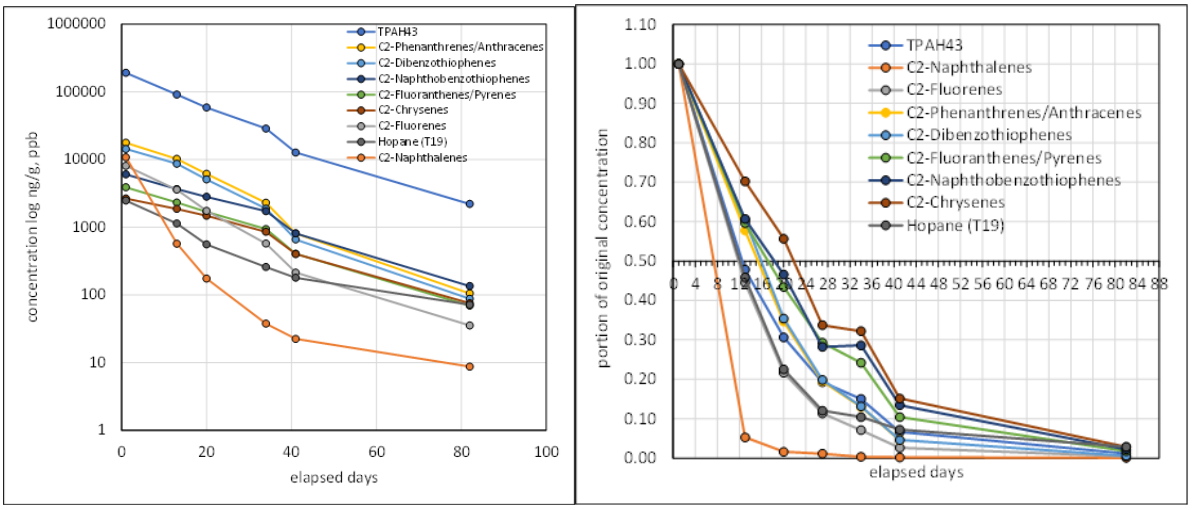

Fig. 5. *Time series of measured and proportional concentrations (left & right plots respectively) for select PAH of forensic interest in spill site mussels. All show log or exponential depletion. Proportional plot (right) estimates half-life (days) at 0.5 axis crossing.*

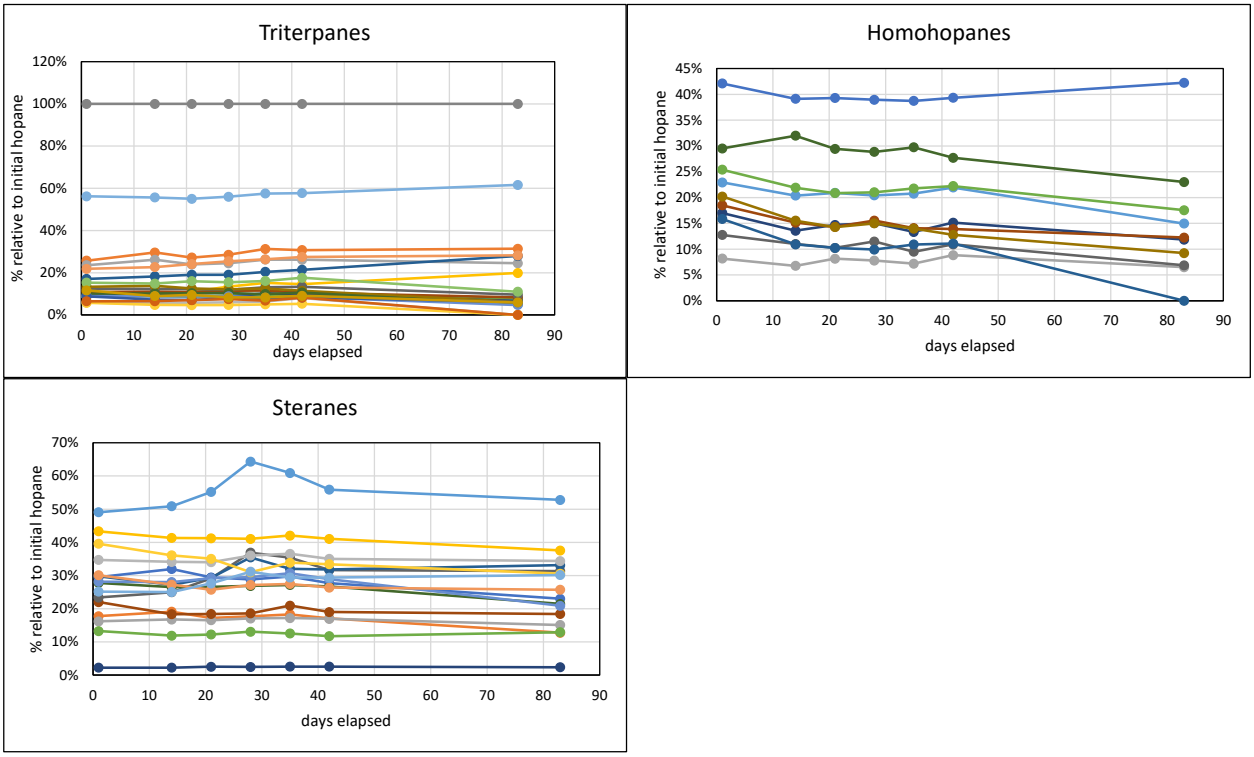

Fig. 6. *Time series of petroleum biomarkers relative to hopane, showing essentially flat or slightly decreasing concentrations.*

3.2. Gene transcription

Transcript patterns were similar across genes for samples taken at multiple time points during the spill event (Fig. 7). Focal genes for this analysis were limited to those thought to be influenced directly by hydrocarbon contamination (see Appendix 1, Table A1-1). These included CASP8, HSP90, MT20, Cyp3, and P53. Of these genes, all except CASP8 exhibited initial levels of transcription (Day 1, 19 days post-spill) that were slightly lower than levels identified in the Port Valdez area 10 months prior to the spill. P53, CASP8, and MT20 then followed a general trend of increasing transcription followed by a decline after study Day 43. HSP90 and Cyp3 patterns were similar, but each had a dip in transcription 21 days after the initial sampling. In the last spill samples taken (Day 83), transcript levels of all genes were trending down towards background levels (LTEMP 2019 and LTEMP 2020).

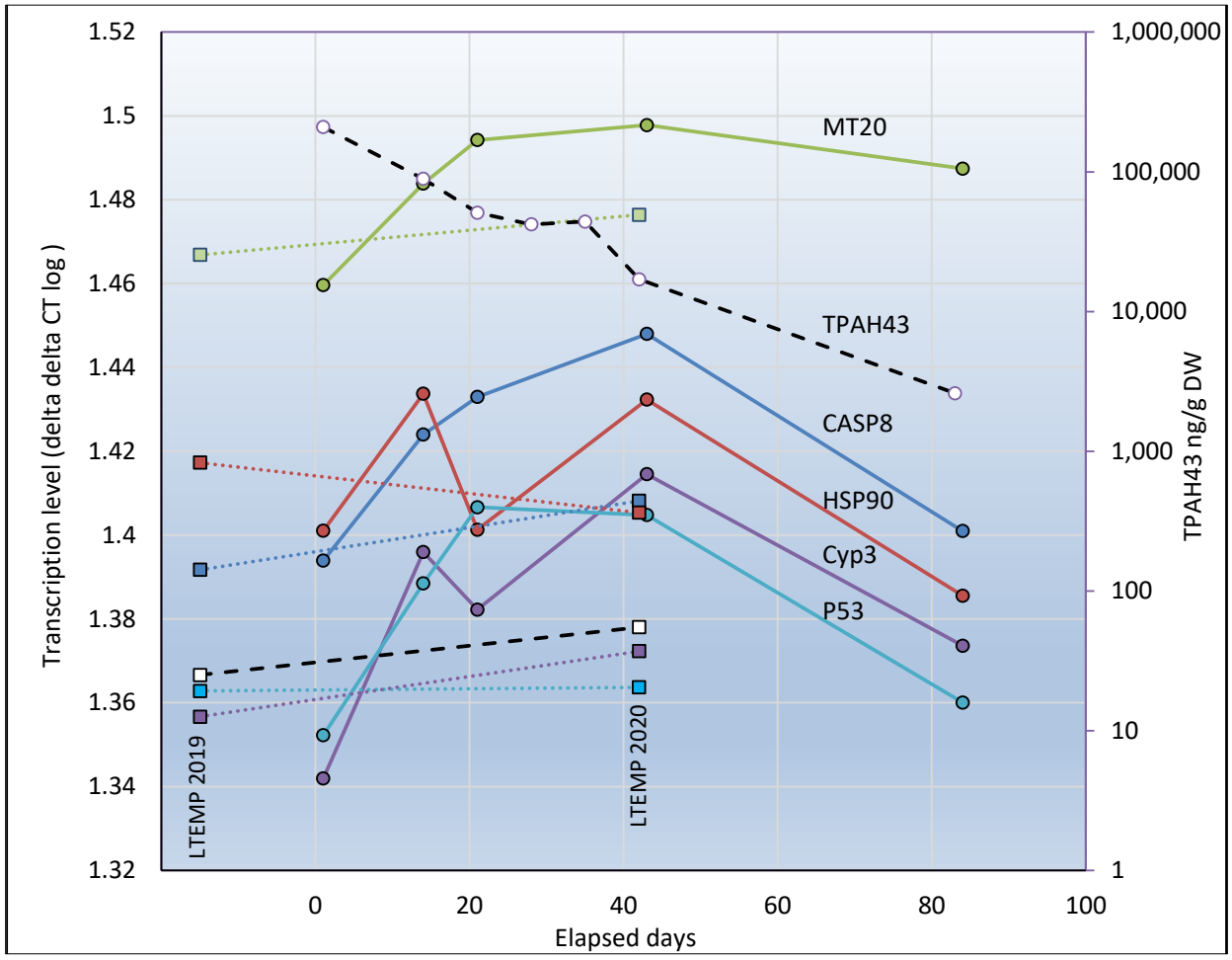

Fig. 7. Transcription levels (CT transformed) of five genes (Table A1-1) directly linked to detoxification and assessed in adductor muscle tissues (solid lines), and tissue TPAH43 concentrations (dashed lines). LTEMP 2019 and 2020 values are from two LTEMP sites (JAP and SAW) and depict average background levels (square symbols connected by dotted lines for genes and by dashed line for TPAH43).

Non-parametric multidimensional scaling (NMDS) was used to compare Port Valdez spill and pre-spill monitoring samples with a 2012-2015 Prince William Sound (PWS) study (Bowen et al., 2018) as a reference (Fig. 8). Two-dimensional NMDS identified a strong separation driven by HSP90, Cyp3, P53, CASP8, and MT20 (Stress = 0.10, R2 = 0.99). PWS samples plotted remote from the spill cluster, while the initial post-spill samples (HZ430) plotted near the non-impacted or "recovered" samples (PV19 and PV20), suggesting that in these initial samples, transcription was suppressed, or these genes were not yet fully activated.

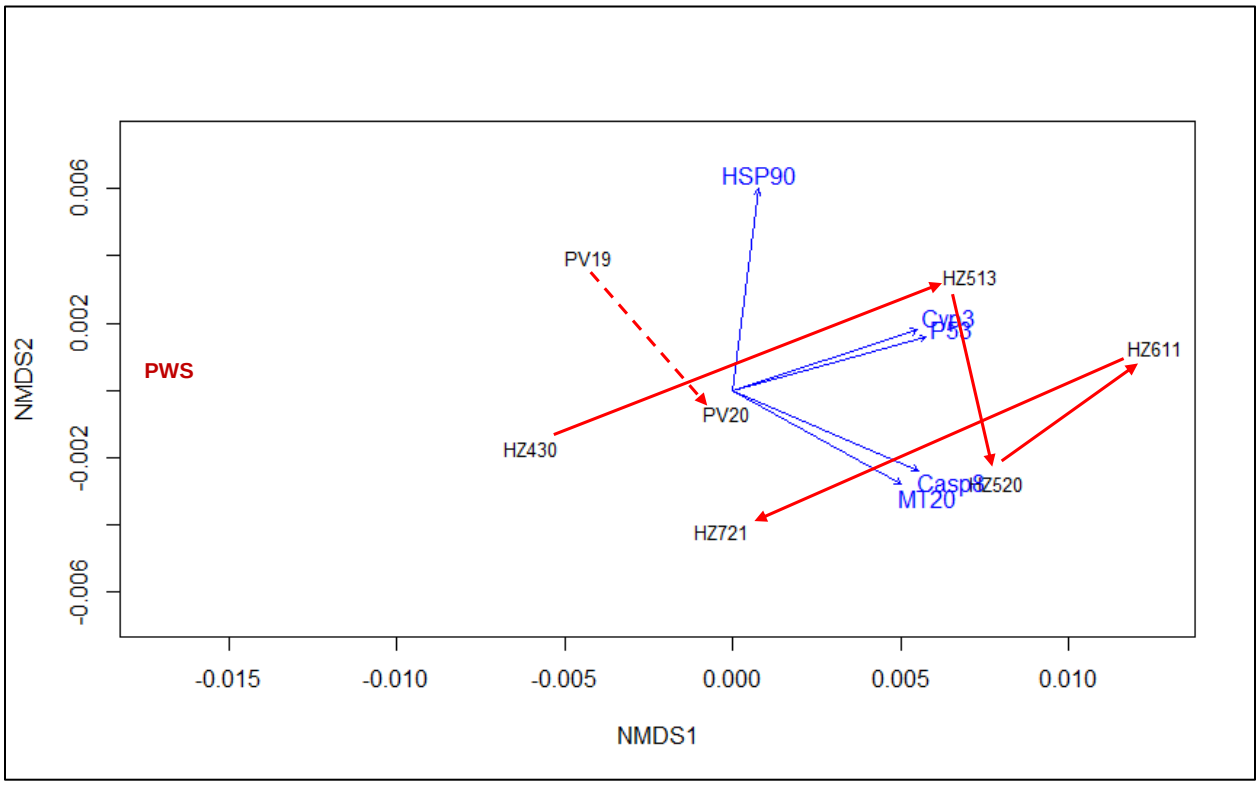

Fig. 8. *Nonparametric, multi-dimensional scaling (NMDS) of mussel gene transcription from the spill zone. Genes included were limited to those directly linked to detoxification processes. Directionality of gene influences are indicated by blue vectors. Spill site samples coded by "HZ" (Hot Zone) plus month/day are connected by red time-sequence arrows to indicate progress of recovery. Port Valdez in 2019 and 2020 (PV19, PV20) represent pre-spill and near-recovery transcription, while Prince William Sound 2012-2015 samples (PWS in red) are included as unexposed regional controls.*

4. Discussion

In general, exposure to ANS crude oil resulted in significant physiological responses in mussel tissues, as indicated by elevated transcription of genes associated with detoxification. These physiological responses persisted even as exposure diminished to relatively lower levels. Essentially, gene transcription levels peaked as hydrocarbon levels were depleting; the timing appeared to lag.

4.1. Chemistry

4.1.1. Profiles

From examining the spill timeline, the monotonically decreasing TPAH43 values and the profiles' weathering-consistent trends (Fig. A4-8), it is reasonable to assume that in the 18-day interval between the initial spill and this study's beginning, oil concentrations in the mussels were higher at some point prior to study Day 1. Thus, these data only address the diminishing exposure towards recovery. The spill-responder accounts (SCAT reports) and our data both suggest that by the end of the study (Day 83), the sheening exposure had not stopped nor had the spill site mussels reached full recovery. The spill site mussels were still above the concentrations seen at the adjacent monitoring sites sampled either mid-study (Day 43, Fig. A4-6) or before the spill (in 2019; Fig. A4-5). Transcription values also show incomplete recovery (discussed below).

PAH and SHC weathering patterns were as expected based mostly on log K_{OW} properties of the individual PAH and microbial preferences for SHC. From previous LTEMP collections, the expected background/recovery point appears as a sparse suite of mixed dissolved and pyrogenic components, each in single digit, ppb concentrations detected at or below MDLs, and without petroleum biomarkers (Fig. A4-5 top panel). Background data from the remote Jack Bay and Galena Bay sites also reflected the trace-level pyrogenic and marine/terrestrial profiles anticipated in these pristine Alaskan intertidal environments (Fig. A4-7).

4.1.2. Depuration

As mentioned above, from depuration calculations, the half-life for the hopane biomarker in mussel tissue was 8.4 days (Fig. 4). This petroleum biomarker is non-biodegradable, essentially not water-soluble (est. log K_{OW} 10-15), and displayed a simple log-decay depletion curve. These characteristics imply it is ingested and eliminated without bioaccumulating, behaving as a simple gut-content tracer (discussed further in Appendix 5). However, the PAH components showed more complexity. PAH that are more lipophilic (higher molecular weights and higher log K_{OW}) are both more easily transported/diffused into body tissues from the gut tract and tend to bioaccumulate. In contrast, the more water-soluble PAH (lower log K_{OW}) tend to absorb as dissolved compounds via the siphon,

mantle, and gills and quickly deplete. Thus, the PAH have different depletion curves whereby they appear to either simply deplete, accumulate in the body tissues, or show some complex mixed-response anomaly (Fig. A5-1).

Seen in PAH depletion plots grouped by the homologous analyte families (parent and alkylated homologs, e.g., fluorene, C1-fluorene, C2-fluorene, and C3-fluorene [F, F1, F2, F3]), and normalized relative to the most recalcitrant PAH, C2-chrysene (C2), the rate of depletion slows with degree of alkylation and increase in log K_{OW} partitioning values (Fig. 5, Fig. A5-1, 4th panel on left). Then a transition occurs. In this study, PAH-depletion curves switch to an accumulation modality that initially appears with the mid-weight, three-ringed PAH, phenanthrene. Here, C4-phenanthrene (PA4) homologue concentration increases in proportion to the sample's C2 over time (Fig. 5-1, 5th panel on left). Seemingly, PAH with log K_{OW} > ~6.3 tended to show bioaccumulation in these mussels (further discussed in Appendix 5; Table A5-1). In contrast, the four-ringed chrysenes are so recalcitrant, it was difficult to characterize the nearly flat depletion curves in the 83-day time series.

There is other disparate behavior in the depletion curves where depletion trends are unexpectedly slower or even flat given the component's log K_{OW}, e.g., C3-fluorene, and all five- and six-ringed, primarily pyrogenic, PAH (Fig. A5-1). The latter are mostly absent in the source oil, so their appearance plus the depletion anomalies suggest that the mussels are chronically re-exposed throughout this study. SCAT reports and communications with agency responders corroborate that light sheening was still present on Day 83.

4.1.3. Transcription

Transcript levels for the selected genes were consistent with a response to oil exposure. Gene transcription profiles associated with the spill show a general trend of initially dampened transcript levels followed by increasing transcription and then, as PAH exposure continued to diminish, a decline in transcript levels to near background levels. Peak levels of transcription were seen at Day 43, at which point the tissue hydrocarbons were already in decline. This concurs with other studies that have detected similar delayed relationships between chemical concentration and transcription, suggesting overwhelmed or inhibited mitigating responses in organisms when initially exposed to high oil concentrations (Poynton and Vulpe, 2009; Garmendia et al., 2011; Pilcher et al., 2014). Two genes (Cyp3 and HSP90) differed slightly from the general trend, with a decline at Day 21. Transcripts of both genes were elevated again by Day 43, with a similar pattern to the other genes thereafter. While the cause of this mid-series decrease in transcription remains unclear, links between HSP90 and Cyp3 are well established (Zhou et al., 2010). PAH bind with the aryl hydrocarbon receptor (AHR), which is chaperoned by HSP90 as the AHR complex is translocated into the nucleus of the cell to bind with the promoter region of cytochrome

P450 genes (Fig. A1-1; Zhou et al., 2010; Murray et al., 2014).

An organism's limited resource budget may contribute to sublethal effects. Continued gene transcription to mitigate stressors, e.g., detoxification, can be physiologically costly (Graham et al., 2010). Long-term chronic or high-concentration, acute oil exposures may overwhelm metabolic pathways while simultaneously causing shifts in resources away from normal cell functions (Portnoy et al., 2020). Stress mitigation imposes extra demands, above those normally required to maintain homeostasis, which may reduce fitness. Fitness loss is usually evidenced by decreased growth and reproductive capability, increased susceptibility to disease, or disadvantageous behavioral changes (Graham et al., 2010; Martin et al., 2010). The individual, and hence the population, suffers.

While gene transcription provides relevant information on physiological status in exposed organisms, synergistic effects among PAH, other potential contaminants, and varying environmental stressors will complicate our interpretations of these physiological responses. For example, PAH exposure initiates gene transcription related to xenobiotic metabolism, but the resulting metabolic products may be toxic (Portnoy et al., 2020). Likewise, temperature, dissolved oxygen, and salinity may all vary in the nearshore marine environment and can influence physiological responses of organisms to chemical exposures (Whitehead, 2013). While the acute effects of oil toxicity are well known (Whitehead, 2013), sublethal effects that are difficult to identify may be critically important for predicting long-term, population-level impacts (Whitehead et al., 2012).

5. Conclusion

In general, transcription results show that following higher levels of tissue PAH burdens, significant physiological responses occurred. Essentially, gene transcription levels peaked as hydrocarbon levels were already partially depleted; the timing appeared lagged. The most probable scenario for these results was that the mussels had limited energy budgets and, as other physiological processes needed the same resources to respond to oil, they were unable to immediately increase transcription of the detoxification genes evaluated in this study.

Additionally, crude oil has been shown to comprise more than thirty-thousand hydrocarbon compounds (McKenna et al., 2013), but current knowledge of bioavailability or toxicity is meager. Traditional PAH-centric toxicity assessments may not be the most relevant values to correlate with transcription response but, pending further research, are the best available proxy.

This has been a limited snapshot of impacted mussels depurating from a single spill in Alaska, in spring and summer, while experiencing diminishing chronic exposures. Though observational, the data show general patterns of oil weathering, depuration and gene transcription that provide multiple lines of evidence for oil exposure, uptake, metabolism, elimination, and impacts in a widely used biomonitoring organism. Further, the study supports a growing area of research that uses gene transcription as a sensitive biomonitoring endpoint for contaminant exposure and physiological responses.

While this study focused on a few genes involved in metabolism and depuration, the next step in this project will be to characterize the entire transcriptome of oiled and unoiled samples to gain a more complete perspective on the activity and scope of oil response.

Credit Authorship Contribution Statement

Lizabeth Bowen: Principal contributions included: transcription analyses and interpretations, synthesis

William B. Driskell: chemistry interpretations, synthesis

James R. Payne: chemistry interpretations, synthesis

Austin Love: project management and field collections

Shannon Waters: Methodology, editing

Eric Litman: chemistry analyses oversight, synthesis

Brenda Ballachey: synthesis

Acknowledgments

Prince William Sound Regional Citizens' Advisory Council provided funding for this research (under Contract #951.21.05 with PECI, and #951.21.07 with the USGS). Any use of trade, firm or product names is for descriptive purposes only and does not imply endorsement by the PWSRCAC or the US Government. Mussel collections were completed under an Aquatic Resources Permit of Alaska Department of Fish and Game (Permit # CF-20-066). Finally, the authors would like to acknowledge the useful review, comments, and suggestions provided by Dr. John W. Farrington, Dean Emeritus, Woods Hole Oceanographic Institution.

References

Apeti, D. A.; Johnson, W. E.; Kimbrough, K. L.; Lauenstein, G. G. 2012. National Status and Trends Mussel Watch Program: Sampling Methods 2012 Update. NOAA Technical Memorandum NOS NCCOS 134; NOAA: Maryland, 2012.

Bodkin, J.; Esler, D.; Rice, S.; Matkin, C.; Ballachey, B. The effects of spilled oil on coastal ecosystems: lessons from the Exxon Valdez spill. In *Coastal Conservation*; Lockwood, J., Maslo, B., Eds.; Cambridge University Press: New York 2014; pp 311-346; DOI 10.1017/CBO9781139137089.013.

Bolognesi, C.; Cirillo, S. Genotoxicity biomarkers in aquatic bioindicators. *Curr. Zool*. 2014, *60*, 273-284; DOI 10.1093/czoolo/60.2.273.

Bowen, L.; Miles, A. K.; Ballachey, B.; Waters, S.; Bodkin, J.; Lindeberg, M.; Esler, D. Gene transcription patterns in response to low level petroleum contaminants in *Mytilus trossulus* from field sites and harbors in southcentral Alaska. *Deep-Sea Res. Part II* 2018, *147*, 27-35; DOI 10.1016/j.dsr2.2017.08.007.

Bustin, S. A.; Benes, V.; Garson, J. A.; Hellemans, J.; Huggett, J.; Kubista, M.; Mueller, R.; Nolan, T.; Pfaffl, M. W.; Shipley, G. L.; Vandesompele, J. The MIQE Guidelines: Minimum information for publication of Quantitative Real-Time PCR experiments. *Clin. Chem.* 2009, *55*, 611-622; DOI 10.1373/clinchem.2008.112797.

Counihan, K. L.; Bowen, L.; Ballachey, B.; Coletti, H.; Hollmen, T.; Pister, B.; Wilson, T. L. Physiological and gene transcription assays to assess responses of mussels to environmental changes. *PeerJ* 2019, *7*, e7800. DOI 10.7717/peerj.7800.

Farr, S.; Dunn, R. T. Concise review: gene expression applied to toxicology. *Toxicol. Sci.* 1999, *50*, 1-9; DOI 10.1093/toxsci/50.1.1.

Garmendia, L.; Soto, M.; Vicario, U.; Kim, Y.; Cajaraville, M. P. Marigómez, I. Application of a battery of biomarkers in mussel digestive gland to assess long-term effects of the Prestige oil spill in Galicia and Bay of Biscay: tissue-level biomarkers and histopathology. *J. Environ. Monit.* 2011, *13,* 915-932; DOI 10.1039/c0em00409j.

Graham, A. L.; Shuker, D. M.; Pollitt, L. C.; Auld, S. K. J. R.; Wilson, A. J.; Little, T. J. Fitness consequences of immune responses: strengthening the empirical framework for ecoimmunology. *Funct. Ecol.* 2010, 25, 1-13; DOI 10.1111/j.1365-2435.2010.01777.x.

Hylland, K. Polycyclic aromatic hydrocarbon (PAH) ecotoxicology in marine ecosystems. *J. Toxicol. Environ. Health, Part A* 2006, *69*, 109-123; DOI 10.1080/15287390500259327.

Incardona, J. P.; Gardner, L. D.; Linbo, T. L.; Brown, T. L.; Esbaugh, A. J.; Mager, E. M.; Stieglitz, J. D.; French, B. L.; Labenia, J. S.; Laetz, C. A.; Tagal, M. Deepwater Horizon crude oil impacts the developing hearts of large predatory pelagic fish. *Proc. Natl. Acad. Sci.* 2014, *111*, E1510–E1518; DOI 10.1073/pnas.1320950111.

Lettieri, T. Recent applications of DNA microarray technology to toxicology and

ecotoxicology. *Environ. Health Persp*. 2006, *114*; DOI 10.1289/ehp.8194.

Livingstone, D. R.; Chipman, J. K.; Lowe, D. M.; Minier, C.; Pipe, R. K. Development of biomarkers to detect the effects of organic pollution on aquatic invertebrates: recent molecular, genotoxic, cellular and immunological studies on the common mussel (*Mytilus edulis* L.) and other mytilids. *Int. J. Environ. Pollut*. 2000, *13*, 56-91; DOI 10.1504/IJEP.2000.002311.

Lowe, R.; Shirley, N.; Bleackley, M.; Dolan, S.; Shafee, T. Transcriptomics technologies. *PLOS Comput. Biol.* 2017, *13*, e1005457. DOI 10.1371/journal.pcbi.1005457.

Martin, L. B.; Hopkins, W. A.; Mydlarz, L. D.; Rohr, J. R. The effects of anthropogenic global changes on immune functions and disease resistance. *Ann. NY Acad. of Sci.* 2010, *1195*, 129-148; DOI 10.1111/j.1749-6632.2010.05454.x.

McKenna, A. M.; Nelson, R. K.; Reddy, C. M.; Savory, J. J.; Kaiser, N. K.; Fitzsimmons, J. E.; Marshall, A. G.; Rodgers, R. P. Expansion of the analytical window for oil spill characterization by ultrahigh resolution mass spectrometry: Beyond gas chromatography. *Environ. Sci. Technol.* 2013, *47*, 7530-7539; DOI 10.1021/es305284t.

McLoughlin, K.; Turteltaub, K.; Bankaitis-Davis, D.; Gerren, R.; Siconolfi, L.; Storm, K.; Cheronis, J.; Trollinger, D.; Macejak, D.; Tryon, V.; Bevilacqua, M. Limited dynamic range of immune response gene expression observed in healthy blood donors using RT-PCR. *Mol. Med*. 2006, *12*, 185-195; DOI 10.2119/2006-00018.mcloughlin.

Murray, I. A.; Patterson, A. D.; Perdew, G. H. Aryl hydrocarbon receptor ligands in cancer: friend and foe. *Nat. Rev. Cancer* 2014, *14,* 801-814; DOI 10.1038/nrc3846.

National Research Council (NRC). Oil in the Sea; Inputs, Fates and Effects. National Academy Press: Washington, D.C., 1985.

Payne, J. R.; Driskell, W. B.; Short, J. W.; Larsen, M. L. Long-term monitoring for oil in the *Exxon Valdez* spill region. *Mar. Pollut. Bull*. 2008, *56*, 2067-2081; DOI 10.1016/j.marpolbul.2008.07.014.

Payne, J.R.; Driskell, W.B. Long-Term Environmental Monitoring Program: 2019 Sampling Results and Interpretations. 2020. Prince William Sound Regional Citizens' Advisory Council.

Payne, J. R.; Driskell, W. B.; Janka, D.; Ka'aihue, L.; Banta, J.; Love, A.; Litman, E. EVOS and the Prince William Sound Long Term Environmental Monitoring Program. In *Proceedings of the 2021 International Oil Spill Conference*, 2021; https://iosc2021.org.

Peterson, C. H.; Rice, S. D.; Short, J. W.; Esler, D.; Bodkin, J. L.; Ballachey, B. E.; Irons, D. B. Long-term ecosystem response to the Exxon Valdez oil spill. *Science* 2003, *302*, 2082-2086; DOI 10.1126/science.1084282.

Pilcher. W.; Miles, S.; Tang, S.; Mayer, G.; Whitehead, A. (2014) Genomic and genotoxic responses to controlled weathered-oil exposures confirm and extend field studies on impacts of the Deepwater Horizon Oil Spill on native killifish. *PLoS ONE* 2014, *9*, e106351. DOI 10.1371/journal.pone.0106351.

Portnoy, D. S.; Fields, A. T.; Greer, J. B.; Schlenk, D. Genetics and oil: transcriptomics, epigenetics, and population genomics as tools to understand animal responses to exposure across different time scales. In *Deep Oil Spills - Facts, Fate, and Effects;* Murawski, A., Ainsworth, C. H., Gilbert, S., Hollander, D. J., Paris, C. B., Schlüter, M., Wetzel, D. L., Eds.; Springer Nature: Switzerland 2020; DOI 10.1007/978-3-030-11605-7_3016.

Poynton, H. C.; Vulpe, C. D. Ecotoxicogenomics: emerging technologies for emerging contaminants. *J. Am. Water Resour. As*. 2009, *45*, 83-96; DOI 10.1111/j.1752-1688.2008.0029.

Snell, T. W.; Brogdon, S. E.; Morgan, M. B. Gene expression profiling in ecotoxicology. *Ecotoxicology* 2003, *12*, 475-483; DOI 10.1023/B:ECTX.0000003033.09923.a8.

Sørhus, E.; Donald, C. E.; Dasilva, D.; Thorsen, A.; Karlsen, O; Meier, S. Untangling mechanisms of crude oil toxicity: linking gene expression, morphology and PAHs at two developmental stages in a cold-water fish. *Sci. Total Environ.* 2020, *757*, 143896. DOI 10.1016/j.scitotenv.2020.143896.

Stout, S. A.; Wang, Z. Chemical fingerprinting methods and factors affecting petroleum fingerprints in the environment. In *Standard Handbook Oil Spill Environmental Forensics: Fingerprinting and Source Identification*, 2nd Edition; Stout, S. A., Wang, Z., Eds.; Academic Press: Massachusetts 2016; pp 1107; DOI 10.1016/B978-0-12-809659 8.00003-6.

Whitehead, A.; Dubansky, B.; Bodinier, C.; Garcia, T. I.; Miles, S.; Pilley, C.; Raghunathan, V.; Roach, J. L.; Walker, N.; Walter, R. B.; Rice, C. D. Genomic and physiological footprint of the Deepwater Horizon oil spill on resident marsh fishes. *P. Natl. A. Sci.* 2012, *109,* 20298-20302; DOI 10.1073/pnas.1109545108.

Whitehead, A. Interactions between oil-spill pollutants and natural stressors can compound ecotoxicological effects. *Integr. Comp. Biol.*, 2013, 53, 635-647; DOI 10.1093/icb/ict080.

Zanette, J.; Jenny, M. J.; Goldstone, J. V.; Parente, T.; Woodin, B. R.; Bainy, A. C.; Stegeman, J. J. Identification and expression of multiple CYP1-like and CYP3-like genes in the bivalve mollusk *Mytilus edulis*. *Aquat. Toxicol*. 2013, *128-129*, 101-112; DOI 10.1016/j.aquatox.2012.11.017.

Zhou, H.; Wu, H.; Liao, C.; Diao, X.; Zhen, J.; Chen, L.; Xue, Q. Toxicology mechanism of the persistent organic pollutants (POPs) in fish through AhR pathway. *Toxicol. Mech. Method* 2010, *20*, 279-286; DOI 10.3109/15376516.2010.485227.

Appendices

Appendix 1: Gene Transcription

Transcription method

Details

As described in Bowen et al. (2018), transcription of 14 genes was used to assess the physiologic status of the mussels; genes used are summarized in Table A1-1. Stability of the proposed reference gene (18S) was determined using the web-based analysis tool RefFinder (Xie et al., 2012). Sufficient stability was found, thus cycle threshold crossing values (C_T) for the genes of interest were normalized to 18S. Although sex can potentially have impacts on gene transcription, most studies investigating gene transcription in the specific genes identified in our panel do not differentiate between sexes (Cellura et al., 2007; Place et al., 2008; Franzellitti et al., 2010; Balseiro et al., 2011; Di et al., 2011; Sureda et al., 2011; Woo et al., 2011; Zeng et al., 2012; Giuliani et al., 2013; Hüning et al., 2013; Woo et al., 2013; Zanette et al., 2013; Lacroix et al., 2014; Châtel et al., 2015; Giannetto et al., 2015), and we did not differentiate by sex in this study.

Tissue collection and RNA extraction

The mussels were kept submerged in seawater and processed as soon as possible following collection, generally within 1-4 h. Gill and adductor muscle tissues were collected from each mussel and placed immediately into RNAlater® (Ambion/Life Technologies, Grand Island, New York). Tissue samples were stored at -20^{0}C. Total RNA was extracted from pulverized gill tissue using the RNeasy Lipid Tissue Mini Kit (Qiagen; http://www.qiagen.com). To remove contaminating genomic (g)DNA, the spin columns were treated with 10 U ml^{-1} of Re-free De I (De, Amersham Pharmacia Biotech Inc.; http://www.apbiotech.com) at -20^{0}C for 15 min. RNA was then stored at -80^{0}C pending further analyses.

cDNA synthesis

A standard cDNA synthesis was performed on 2 mg of RNA template from each mussel. Reaction conditions included 4 units reverse transcriptase (Omniscript, Qiagen, Valencia, CA, USA), 1 mM random hexamers, 0.5 mM each dNTP, and 10 units Re inhibitor, in RT buffer (Qiagen, Valencia, CA, USA). Reactions were incubated for 60 min at 37^{0}C, followed by an enzyme inactivation step of 5 min at 93^{0}C, and then stored at -20^{0}C until further analysis.

Real-time PCR

Real-time PCR reactions for the individual genes of interest and the housekeeping gene (18S) were run in separate wells (Bowen et al., 2018). Briefly, 1 ml of cDNA was added to a mix containing 12.5 ml of QuantiTect Fast SYBR GreenR Master Mix (5 mM Mg 2C) (Qiagen, Valencia, CA, USA), 0.5 ml each of forward and reverse sequence specific primers (Invitrogen, Carlsbad, CA, USA), and 10.5 ml of Re-free water; total reaction mixture was 25 ml. The reaction mixture cDNA samples for each gene of interest and 18S were loaded into Fast 96 well plates in duplicate and sealed with optical sealing tape (Applied Biosystems, Foster City, CA, USA). Reaction mixtures that contained water but no cDNA were used as negative controls.

Statistical analysis

Analyses of qPCR data were conducted using normalized C_T values (housekeeping gene threshold crossing subtracted from the gene of interest threshold crossing); the lower the normalized value, the more transcripts are present. A change in normalized value of 2 is approximately equivalent to a 4-fold change in the amount of the transcript. A normalized value of 34 or higher indicated a quantity less than the detection limit for transcription of that gene. C_T values were converted to relative load using the 2^(-C_T') method (Livak and Schmittgen, 2001), and then log-transformed. We conducted multivariate, non-parametric, multi-dimensional scaling analysis (NMDS; R 2013) in conjunction with cluster analysis on the log transformed data for statistical and graphical representation of individual mussels clustered by similarity in transcript pattern.

Table A1-1. Genes selected for the mussel transcription panel and their primary functions and interactions.

Gene	Function	Environmental interaction parameter
Calmodulin (CaM)	CaM has been reported as a pivotal calcium metabolism regulator in shell formation, and also responds to a wide range of stressors including ocean acidification, increased temperatures and decreased available oxygen (Li et al., 2004; Woo et al., 2011; Chen et al., 2012; Zeng et al., 2012).	Ocean acidification Temperature Dissolved oxygen
Caspase 8 (CASP8)	Caspases play essential roles in apoptosis (programmed cell death), necrosis, and inflammation. The apoptotic process could be tightly regulated in bivalve mollusks by overexpression/suppression of caspase genes; additionally, there is evidence of caspase-specific responses to pathogens and pollutants (Romero et al., 2011; Lacroix et al., 2014).	Pathogens Contaminants
Macrophage migration inhibitory factor (MIF)	MIF is an important mediator of the innate immune system as evidenced by its response to pathogen challenge (Balseiro et al., 2011).	Pathogens
Calponin (CNN)	CNN, a calcium-binding molecule, has been shown to be significantly reduced in the absence of sufficient oxygen (Hüning et al., 2013).	Ocean acidification Dissolved oxygen
Chitinase (CHI)	In mussels and other marine invertebrates, CHI plays a role in digestion and in the control of growth and remodeling processes (Banni et al., 2011). CHI transcription has been shown to decrease with decreasing levels of available oxygen (Woo et al., 2011; Hüning et al., 2013).	Ocean acidification Dissolved oxygen
Cytochrome C Oxidase IV (CCOIV)	Under conditions of reduced O_2 availability, hypoxia-inducible factor 1 (HIF-1) reciprocally regulates Cytochrome C Oxidase IV (CCOIV) subunit expression by	Dissolved oxygen

	activating transcription of the gene encoding CCOIV. The CCOIV subunit optimizes the efficiency of respiration at different O_2 concentrations (Fukuda et al., 2007; Woo et al., 2011; Woo et al., 2013).	
Heat shock proteins 70 and 90 (HSP70 and HSP90)	Heat shock proteins are produced in response to exposure to different kinds of environmental stress conditions, such as infection, inflammation, exposure to contaminants, hypoxia, thermal or other stress (Iwama et al., 1999; Tsan and Gao, 2004). In addition to being expressed in response to a wide array of stressors, heat shock proteins act as molecular chaperone (De Maio, 1999) facilitating contaminant transfer across cell walls and into the nucleus.	Temperature Pathogens Contaminants
Hypoxia-inducible factor alpha (HIFa)	HIFs are transcription factors that respond to changes in available oxygen in the cellular environment, specifically to decreases in oxygen, or hypoxia (Wu, 2002; Giannetto et al., 2015).	Dissolved oxygen
Myticin B (MytB)	MytB is an antimicrobial peptide that has a broad range of actions against many microorganisms including viruses, bacteria, and fungi. In marine invertebrates, antimicrobial peptides are the leading elements of the immune response (Balseiro et al., 2011).	Pathogens
Mytilin (Myt)	Myt is an antimicrobial peptide that plays an important role in innate immunity and a prominent role in killing intracellular bacteria after phagocytosis (Mitta et al., 2000). Transcription of Myt has also been shown to increase with decreasing ocean pH (Hüning et al., 2013).	Pathogens
Metallothionein 20 (MT20)	MT20 is an important component of the detoxification system; transcription of MT20 increases in the presence of hydrocarbons as well as metals (Banni et al., 2007; Franzellitti et al., 2010; Sureda et al., 2011; Lacroix et al., 2014;).	Contaminants - metals
Cytochrome P450, family 3 (Cyp3)	Cyp3 is an important component of the general detoxification system; transcription of Cyp3 increases in the presence of contaminants (Giuliani et al., 2013; Zanette et al., 2013).	Contaminants

Tumor protein 53 (p53)	P53 is known to be involved in development, differentiation, cell response and stress (Bourdon, 2007). It has been documented that in invertebrates, p53 has a role in apoptosis and cell death (Goodson et al., 2006). Transcription of p53 has been shown to increase in the presence of PAHs (Di et al., 2011).	Contaminants - PAHs

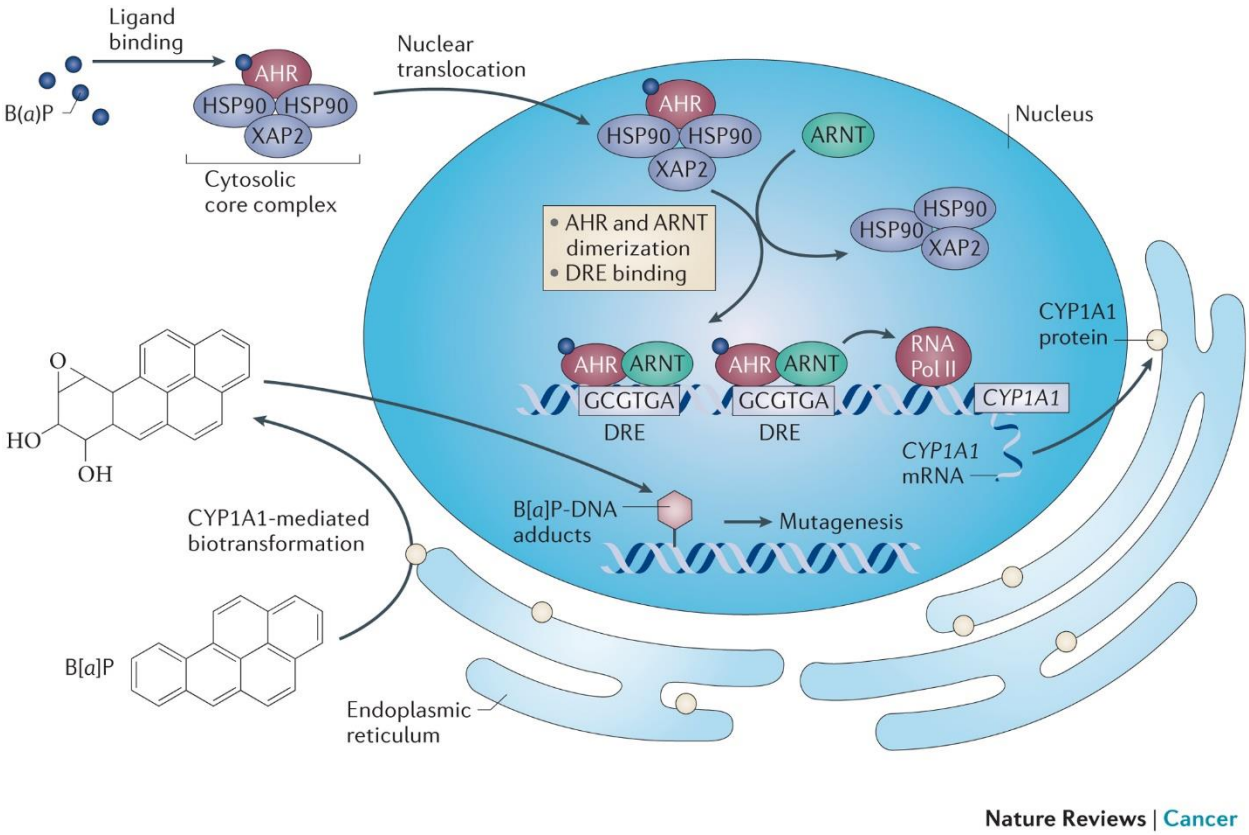

Fig. A1-1*. In the context of our study, this figure illustrates the close relationship between HSP90 and Cyp3, a member of the cytochrome P450 family, which includes CYP1A1. In the broader context, the aryl hydrocarbon receptor (AHR) is complexed with HSP90 and its co-chaperone, XAP2. Upon binding an agonist (in this case, the PAH benzo[a]pyrene), the AHR complex moves into the nucleus where transcription of CYP1A1 is activated. The AHR target gene CYP1A1 is almost totally dependent on AHR activity for transcription and is highly induced by AHR activation. CYP1A1 metabolizes a number of pro-carcinogens, such as PAH, to intermediates that can react with DNA to form adducts, resulting in subsequent mutagenesis (Murray et al., 2014). Reprinted by permission from Copyright Clearance Center: (Springer Nature) [Nature Reviews Cancer] REFERENCE CITATION (Aryl hydrocarbon receptor ligands in cancer: friend and foe, Iain A. Murray et al.), [COPYRIGHT]* (2014).

Table A1-2. Median gene transcription values associated with study locations and timepoints. C_T values were converted to relative load using the 2^(-C_T') method (Livak and Schmittgen, 2001), and then log-transformed. Gene abbreviations are defined above in Table A1-1.

Location	CaM	CASP8	MIF	CNN	CHI	CCOIV	HSP70	HSP90	HIFa	MytB	Myt	MT20	Cyp3	P53
PV19	1.27	1.38	1.31	1.25	1.27	1.22	1.43	1.42	1.40	1.38	1.29	1.47	1.35	1.37
HZ430	1.29	1.39	1.31	1.26	1.31	1.28	1.42	1.40	1.38	1.34	1.32	1.46	1.34	1.35
HZ513	1.31	1.42	1.38	1.31	1.32	1.29	1.43	1.43	1.39	1.48	1.37	1.48	1.40	1.39
HZ520	1.33	1.43	1.32	1.34	1.30	1.32	1.45	1.40	1.41	1.49	1.38	1.49	1.38	1.41
HZ611	1.33	1.45	1.33	1.34	1.32	1.33	1.45	1.43	1.40	1.44	1.36	1.50	1.41	1.40
HZ721	1.26	1.40	1.34	1.31	1.28	1.23	1.42	1.39	1.39	1.46	1.33	1.49	1.37	1.36
PWS	1.30	1.36	1.33	1.26	1.29	1.24	1.44	1.41	1.39	1.40	1.32	1.40	1.34	1.33
PV20	1.29	1.41	1.31	1.31	1.31	1.27	1.42	1.40	1.38	1.38	1.34	1.48	1.37	1.37

Appendix 2: Hydrocarbon Analytic Methods

Laboratory Methods

Collection and analytical methods are generally patterned after the NOAA Mussel Watch Program but with analytic updates (Payne et al., 2006). Briefly, three replicates of 30 mussels are collected by hand at each site. Analyses were provided by Alpha Analytical Laboratory (Mansfield, MA) under the guidance of NewFields Environmental Forensics Practice (Rockland, MA).

The usual suite of oil hydrocarbon data is reported: polycyclic aromatic hydrocarbons (PAH), saturated hydrocarbons (SHC), and sterane/triterpane petroleum biomarkers (S/T). As semi-volatile compounds, the PAH, alkylated PAH, and petroleum biomarkers, are analyzed using selected ion monitoring gas chromatography/mass spectrometry (SIM GC/MS) via a modified Environmental Protection Agency (EPA) Method 8270 (aka 8270M). This analysis provides the concentration of 1) approximately 80 PAH, alkylated PAH homologues, individual PAH isomers, and sulfur-containing aromatics and 2) approximately 50 tricyclic and pentacyclic triterpanes, regular and rearranged steranes, and triaromatic and monoaromatic steroids. Complete lists of PAH, SHC, and biomarker (S/T) analytes are presented below along with the analyte abbreviations used in figures throughout this paper.

Using a modified EPA Method 8015B, SHC are quantified as total extractable materials (TEM; C_9-C_{44}) and as concentrations of n-alkanes (n-C_9 to n-C_{40}) and selected (C_{15}-C_{20}) acyclic isoprenoids (e.g., pristane and phytane). A high-resolution gas chromatography/flame ionization detector (GC/FID) fingerprint of each sample is also provided along with the lab sample processing and analytic documentation.

Hydrocarbon Analytes

Polycyclic aromatic hydrocarbons (PAH)

Analytes	Abbreviation
Naphthalene	N
C1-Naphthalene	N1
C2-Naphthalene	N2
C3-Naphthalene	N3
C4-Naphthalene	N4
Biphenyl	BI
Acenaphthylene	ACY
Acenaphthene	ACN
Fluorene	F
C1-Fluorene	F1
C2-Fluorene	F2
C3-Fluorene	F3
C4-Fluorene	F4
Anthracene	A
Phenanthrene	Ph
C1-Phenanthrene/Anthracene	PA1
C2-Phenanthrene/Anthracene	PA2
C3-Phenanthrene/Anthracene	PA3
C4-Phenanthrene/Anthracene	PA4
Retene	RET
Dibenzothiophene	DBT
C1-Dibenzothiophene	DBT1
C2-Dibenzothiophene	DBT2
C3-Dibenzothiophene	DBT3
C4-Dibenzothiophene	DBT4
Benzo(b)fluorene	BF

Analytes	Abbreviation
Fluoranthene	FL
Pyrene	PY
C1-Fluoranthene/Pyrene	FP1
C2-Fluoranthene/Pyrene	FP2
C3-Fluoranthene/Pyrene	FP3
C4-Fluoranthene/Pyrene	FP4
Napthobenzothiophene	NBT
C1-Napthobenzothiophene	NBT1
C2-Napthobenzothiophene	NBT2
C3-Napthobenzothiophene	NBT3
C4-Napthobenzothiophene	NBT4
Benzo(a)Anthracene	BAA
Chrysene	C
C1-Chrysene	C1
C2-Chrysene	C2
C3-Chrysene	C3
C4-Chrysene	C4
Benzo(b)fluoranthene	BBF
Benzo(k)fluoranthene	BKF
Benzo(e)pyrene	BEP
Benzo(a)pyrene	BAP
Perylene	PER
Indeno(1,2,3-cd)pyrene	IND
Dibenzo(a,h)anthracene	DAHA
Benzo(g,h,i)perylene	BGH
Total PAH	TPAH

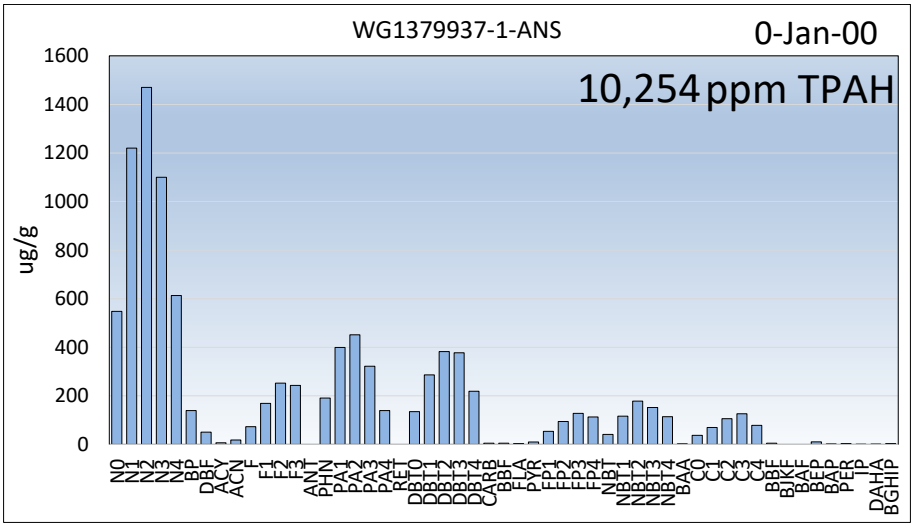

ANS Crude oil example

Saturated hydrocarbons (SHC or n-alkanes)

Analyte	Abbrev
Nonane (C9)	C9
Decane (C10)	C10
Undecane (C11)	C11
Dodecane (C12)	C12
Tridecane (C13)	C13
2,6,10 Trimethyldodecane (1380)	1380
Tetradecane (C14)	C14
2,6,10-Trimethyltridecane (1470)	1470
Pentadecane (C15)	C15
Hexadecane (C16)	C16
Norpristane (1650)	Pristane
Heptadecane (C17)	C17
Pristane	Phytane
Octadecane (C18)	C18
Phytane	Phy
Nonadecane (C19)	C19
Eicosane (C20)	C20
Heneicosane (C21)	C21
Docosane (C22)	C22
Tricosane (C23)	C23
Tetracosane (C24)	C24
Pentacosane (C25)	C25
Hexacosane (C26)	C26
Heptacosane (C27)	C27
Octacosane (C28)	C28
Nonacosane (C29)	C29
Triacontane (C30)	C30
Hentriacontane (C31)	C31
Dotriacontane (C32)	C32
Tritriacontane (C33)	C33
Tetratriacontane (C34)	C34
Pentatriacontane (C35)	C35
Hexatriacontane (C36)	C36
Heptatriacontane (C37)	C37
Octatriacontane (C38)	C38
Nonatriacontane (C39)	C39
Tetracontane (C40)	C40
Total SHC	TSHC

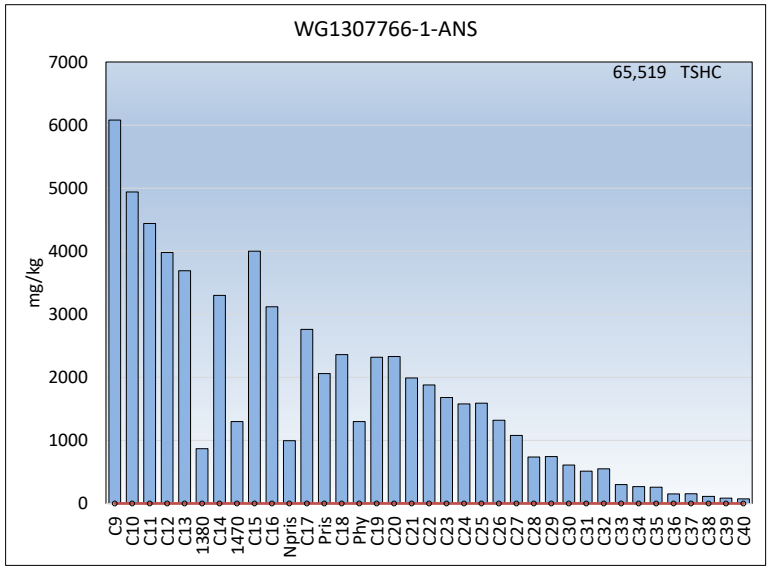

Petroleum Biomarkers (S/T)

Class	Biomarker	Abbrev
Terpanes	C23 Tricyclic Terpane (T4)	T4
	C24 Tricyclic Terpane (T5)	T5
	C25 Tricyclic Terpane (T6)	T6
	C24 Tetracyclic Terpane (T6a)	T6a
	C26 Tricyclic Terpane-22S	T6b
	C26 Tricyclic Terpane-22R	T6c
	C28 Tricyclic Terpane-22S (T7)	T7
	C28 Tricyclic Terpane-22R (T8)	T8
	C29 Tricyclic Terpane-22S (T9)	T9
	C29 Tricyclic Terpane-22R	T10
	18a-22,29,30-	Ts
	C30 Tricyclic Terpane-22S	C30Ts
	C30 Tricyclic Terpane-22R	C30Tr
opanes	17a(H)-22,29,30-	Tm
	17a/b,21b/a 28,30-	14a
	17a(H),21b(H)-25-Norhopane	14b
	30-Norhopane (T15)	T15
	18a(H)-30-Norneohopane-	T16
	17a(H)-Diahopane (X)	X
	30-Normoretane (T17)	T17
	18a(H)&18b(H)-Oleananes	T18
	Hopane (T19)	T19*
	Moretane (T20)	T20
	30-Homohopane-22S (T21)	T21
	30-Homohopane-22R (T22)	T22
	Gammacerane/C32-	T22a
	30,31-Bishomohopane-22S	T26
	30,31-Bishomohopane-22R	T27
	30,31-Trishomohopane-22S	T30
	30,31-Trishomohopane-22R	T31
	Tetrakishomohopane-22S	T32
	Tetrakishomohopane-22R	T33
	Pentakishomohopane-22S	T34
	Pentakishomohopane-22R (T35)	T35
Steranes	13b(H),17a(H)-20S-Diacholestane (S4)	S4
	13b(H),17a(H)-20R-Diacholestane (S5)	S5

Class	Biomarker	Abbrev
	13b,17a-20S-Methyldiacholestane (S8)	S8
	17a(H)20SC27/C29dia	DIA29S
	17a(H)20rc27/C29dia	DIA29R
	Unknown Sterane (S18)	S18
	13a,17b-20S-Ethyldiacholestane (S19)	S19
	14a,17a-20S-Methylcholestane (S20)	S20
	14a,17a-20R-Methylcholestane (S24)	S24
	14a(H),17a(H)-20S-Ethylcholestane (S25)	S25
	14a(H),17a(H)-20R-Ethylcholestane (S28)	S28
	14b(H),17b(H)-20R-Cholestane (S14)	S14
	14b(H),17b(H)-20S-Cholestane (S15)	S15
	14b,17b-20R-Methylcholestane (S22)	S22
	14b,17b-20S-Methylcholestane (S23)	S23
	14b(H),17b(H)-20R-Ethylcholestane (S26)	S26
	14b(H),17b(H)-20S-Ethylcholestane (S27)	S27
	C20 Pregnane	Preg
	C21 20-Methylpregnane	MPreg
	C22 20-Ethylpregnane (a)	EPregA
	C22 20-Ethylpregnane (b)	EPregB
Triaromatic Steroids	C26,20S TAS	TAS0
	C26,20R+C27,20S TAS	TAS1
	C28,20S TAS	TAS2
	C27,20R TAS	TAS3
	C28,20R TAS	TAS4
	C29,20S TAS	TAS5
	C29,20R TAS	TAS6
Mono-aromatic Steroids	5b(H)-C27 (20S) MAS+	MAS1
	5b(H)-C27 (20R) MAS+	MAS2

Class	Biomarker	Abbrev
	5a(H)-C27 (20S) MAS	MAS3
	5b(H)-C28 (20S) MAS+	MAS4
	5a(H)-C27 (20R) MAS	MAS5
	5a(H)-C28 (20S) MAS	MAS6
	5b(H)-C28 (20R) MAS+	MAS7
	5b(H)-C29 (20S) MAS+	MAS8
	5a(H)-C29 (20S) MAS	MAS9
	5a(H)-C28 (20R) MAS	MAS10
	5b(H)-C29 (20R) MAS+	MAS11
	5a(H)-C29 (20R) MAS	MAS12

*hopane highlighted gold in plots

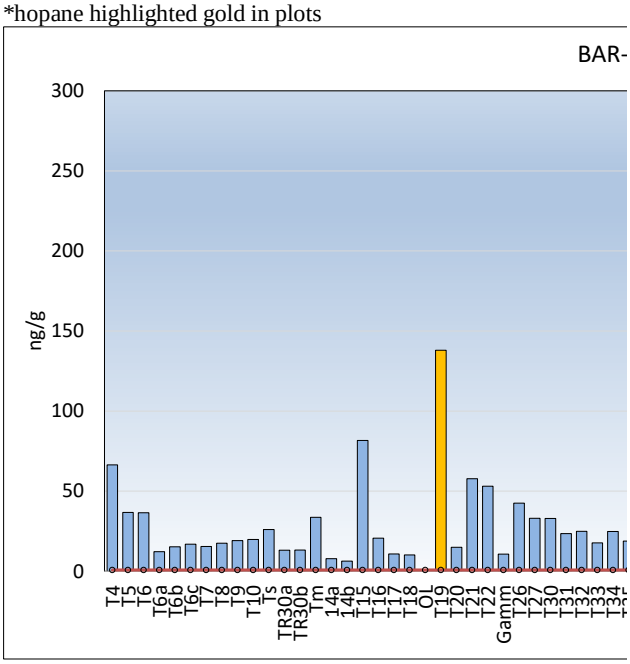

ANS spill oil from 2017

Laboratory Quality Control

All Alpha/NewFields-analyzed constituents are reported on a ng/g dry weight (DW) basis uncorrected for blanks or surrogate recoveries. Surrogates are novel or deuterated compounds added in known amounts to each raw sample to assess, by their final percent recovery, the efficiency of extraction and analysis. Surrogate recoveries are considered acceptable if they are between 40% and 120%. A single recovery deviance flags the sample with cautionary remarks; multiple recovery deviations would require batch reanalysis. Surrogate recovery standards were met for all PAH, biomarker and alkane surrogate hydrocarbons analyzed during the 2020 reporting period (Table A2-1). Laboratory method blanks for each analytic sample batch demonstrated (sub-ng/g) laboratory or analytic background PAH interference.

***Table A2-1**. Surrogate recovery statistics from 2020 Alpha Laboratory analyses.*

Surrogate	Average (%)	Max	Min	Count	StdDev
5B(H)Cholane	97	109	87	25	6
Benzo[a]pyrene-d12	83	94	73	29	5
d50-Tetracosane	91	101	81	24	5
Naphthalene-d8	64	76	55	29	6
Phenanthrene-d10	80	91	74	29	3

Method Detection Limits

Alpha Analytical Laboratory's MDLs for hydrocarbons exceed the performance of most commercial labs, falling within the accepted stricter levels for forensic purposes (Table A2-2).

***Table A2-2**. Alpha Analytical MDL target ranges.*

Analytes	Tissue (15 g sample)	Oil Reporting Level (RL)
PAH and biomarkers	0.2-1.0 ng/g Dry Wt.	2.0 µg/g
SHC	0.01-0.08 µg/g Dry Wt.	200 µg/g

Appendix 3: Hydrocarbon Sample Plots

This appendix contains PAH, SHC and petroleum (S/T) biomarker plots for all samples and replicates analyzed for this paper. Tissue PAH and S/T concentrations are reported in ppb on dry-weight basis; tissue SHC and oil as ppm. Red lines represent sample-weight-adjusted method detection limits (MDL) for each analyte. Values below MDL are reported as estimated quantities but are considered to have interpretive significance. Non-detects are reported as zeroes. The gold-highlighted petroleum biomarker is hopane (T19). Some sample replicates were not analyzed for SHC and thus, appear blank.

Source oil (ppm) – 1 May 2020

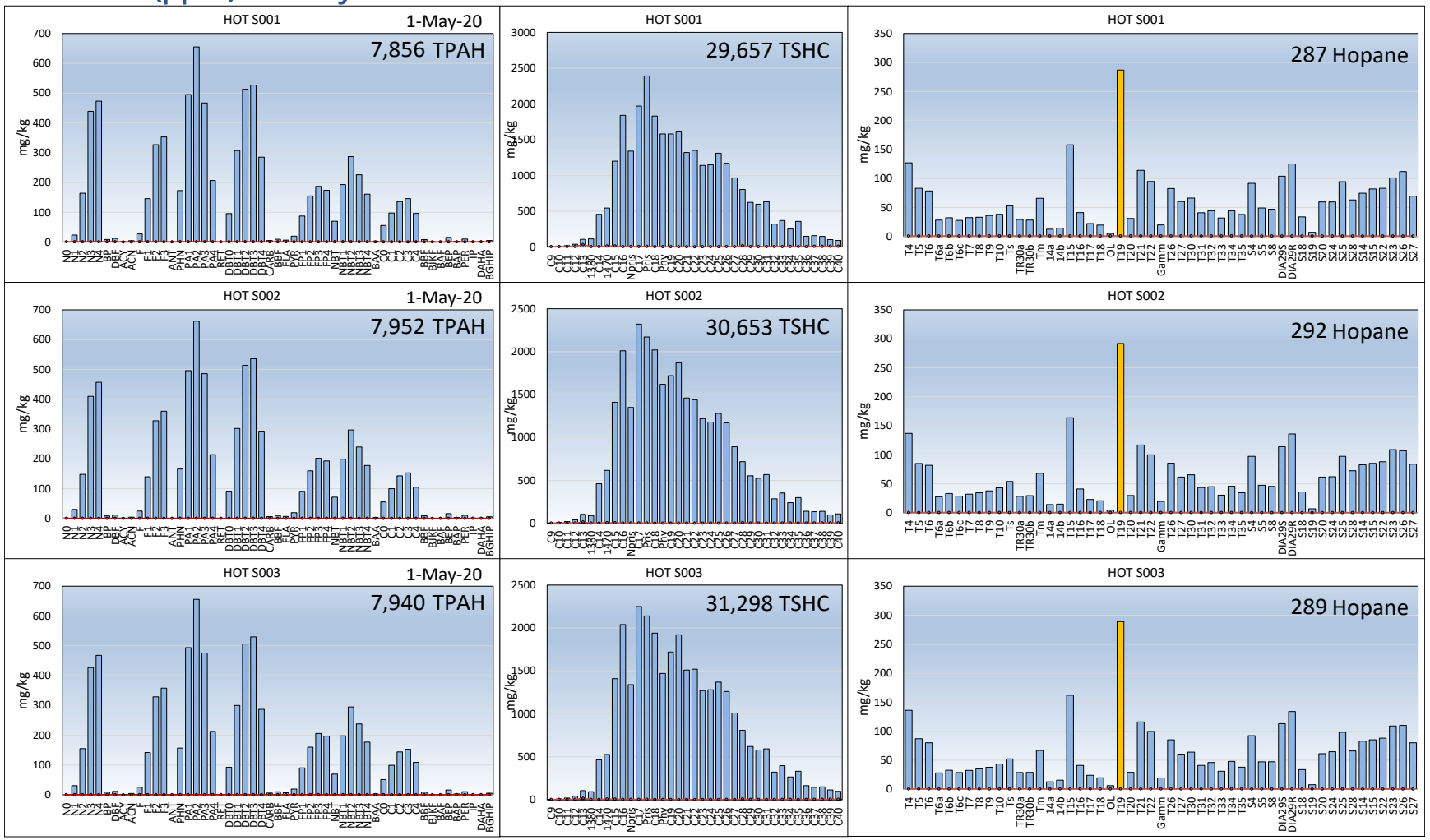

Spill site (Hot Zone) mussel tissues (PAH and S/T, ppb; SHC ppm) – 30 April

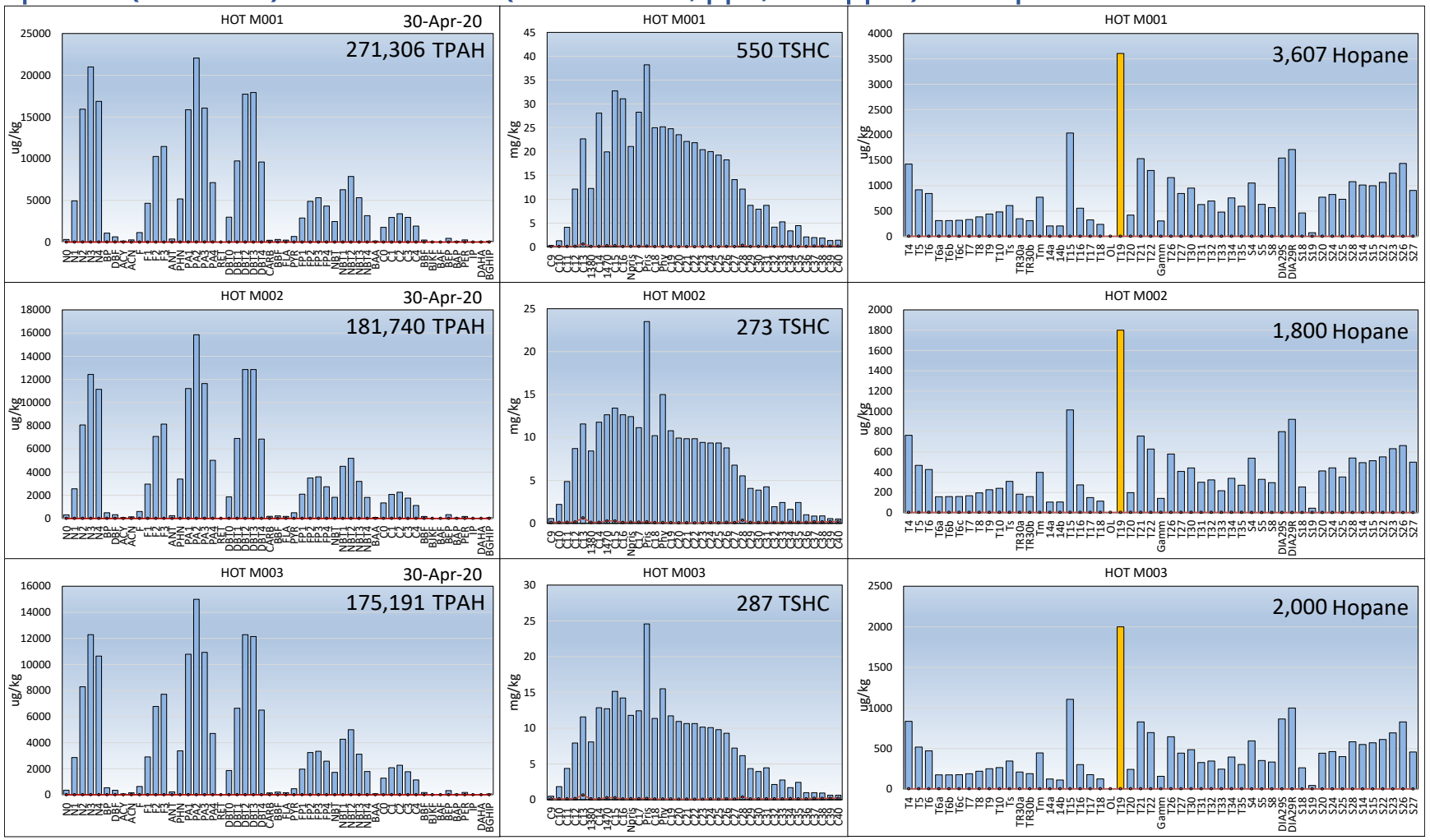

Spill site (Hot Zone) mussel tissues (PAH and S/T, ppb; SHC ppm) – 13 May

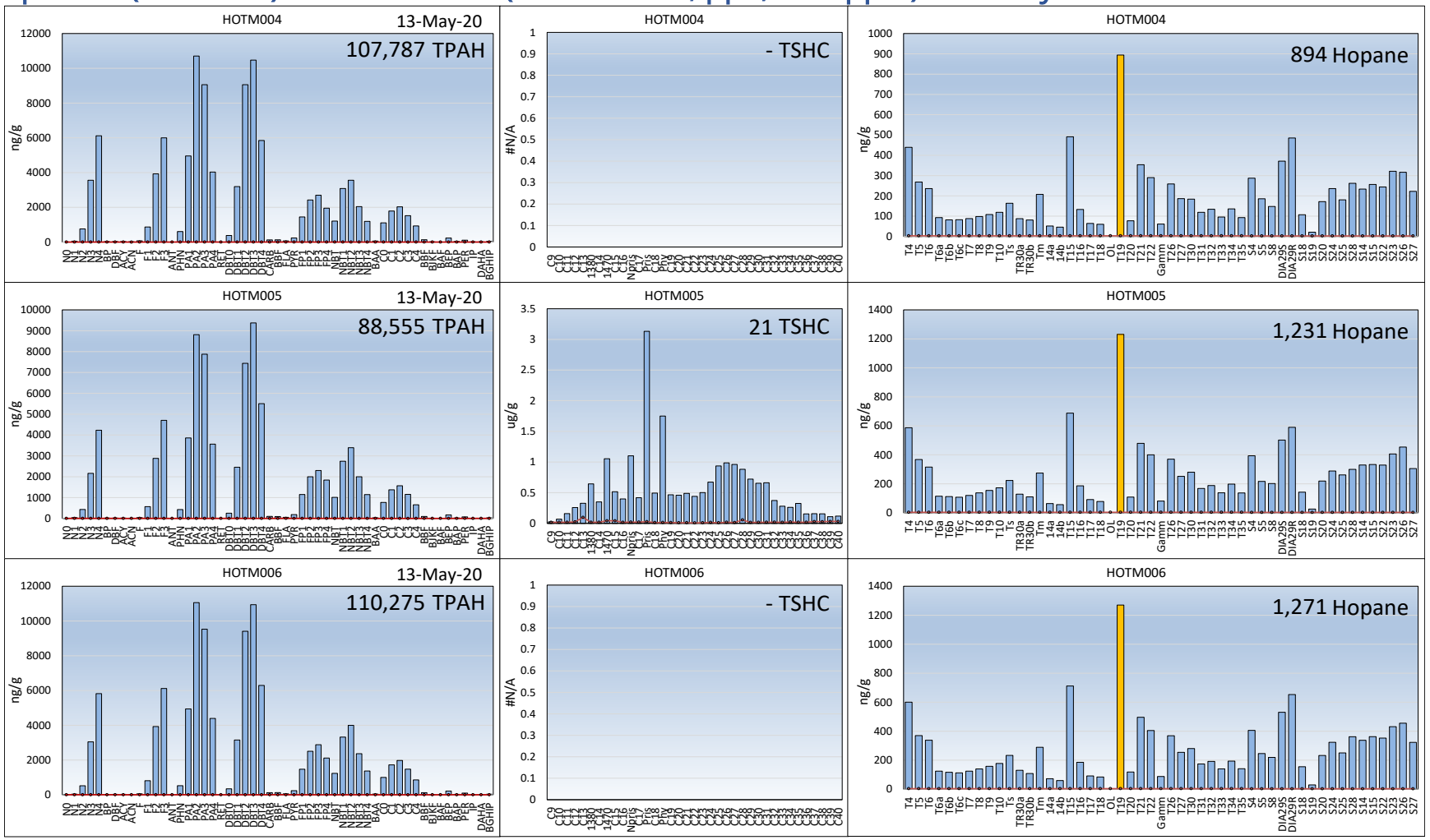

Spill site (Hot Zone) mussel tissues (PAH and S/T, ppb; SHC ppm) – 20 May

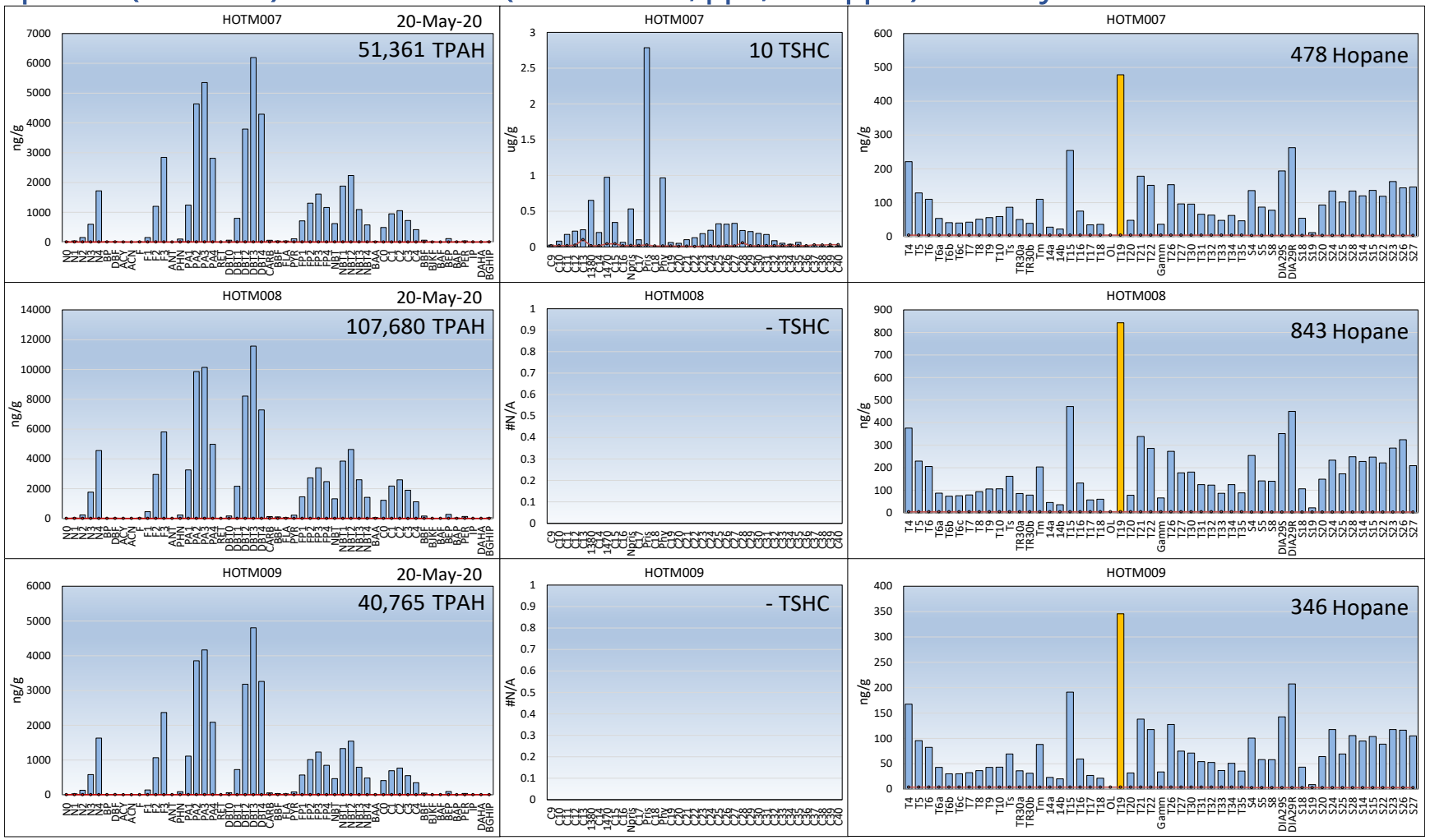

Spill site (Hot Zone) mussel tissues (PAH and S/T, ppb; SHC ppm) – 27 May

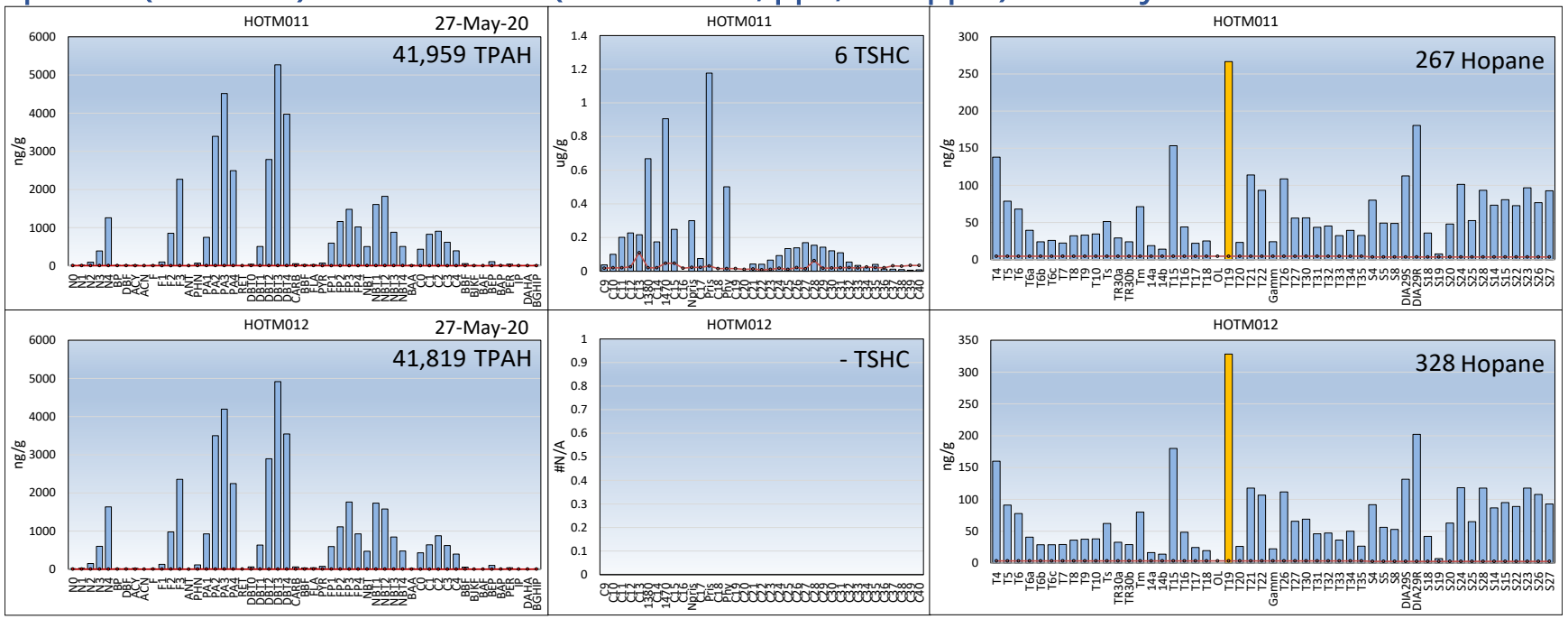

Spill site (Hot Zone) mussel tissues (PAH and S/T, ppb; SHC ppm) – 3 June

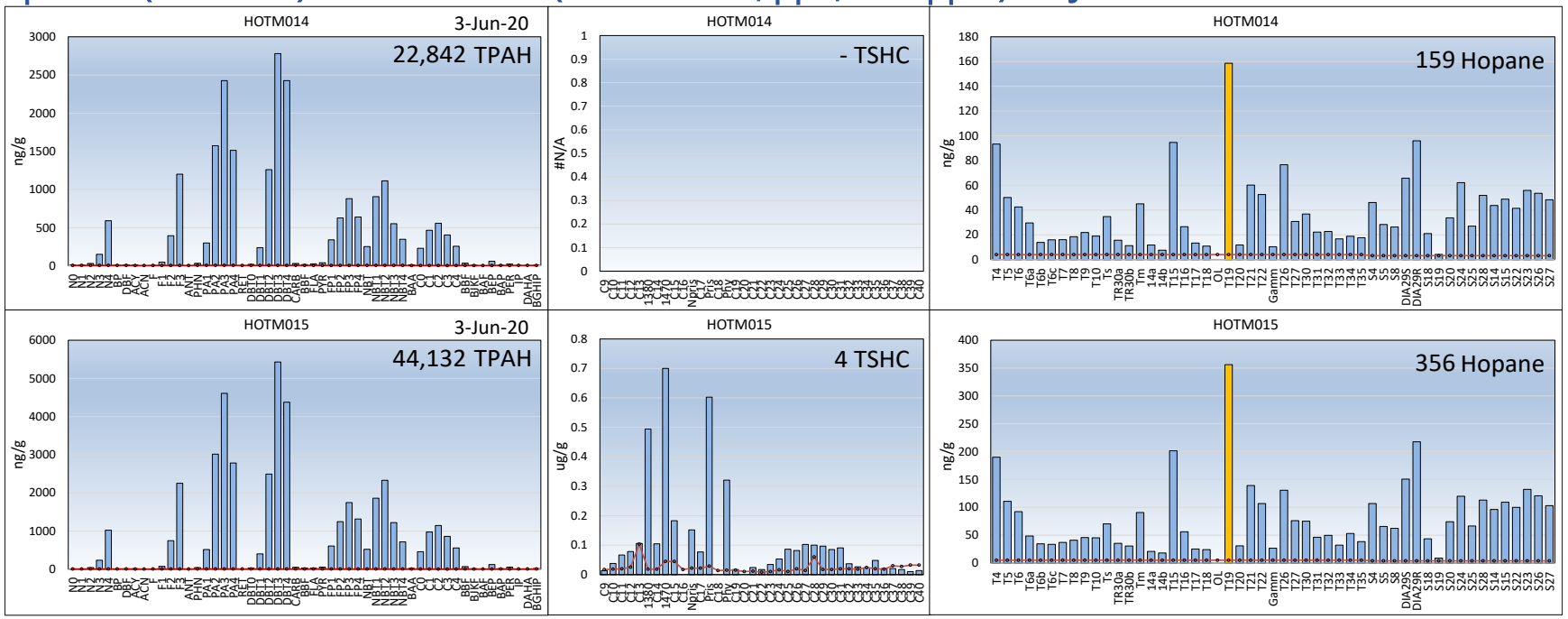

Spill site (Hot Zone) mussel tissues (PAH and S/T, ppb; SHC ppm) – 10 June

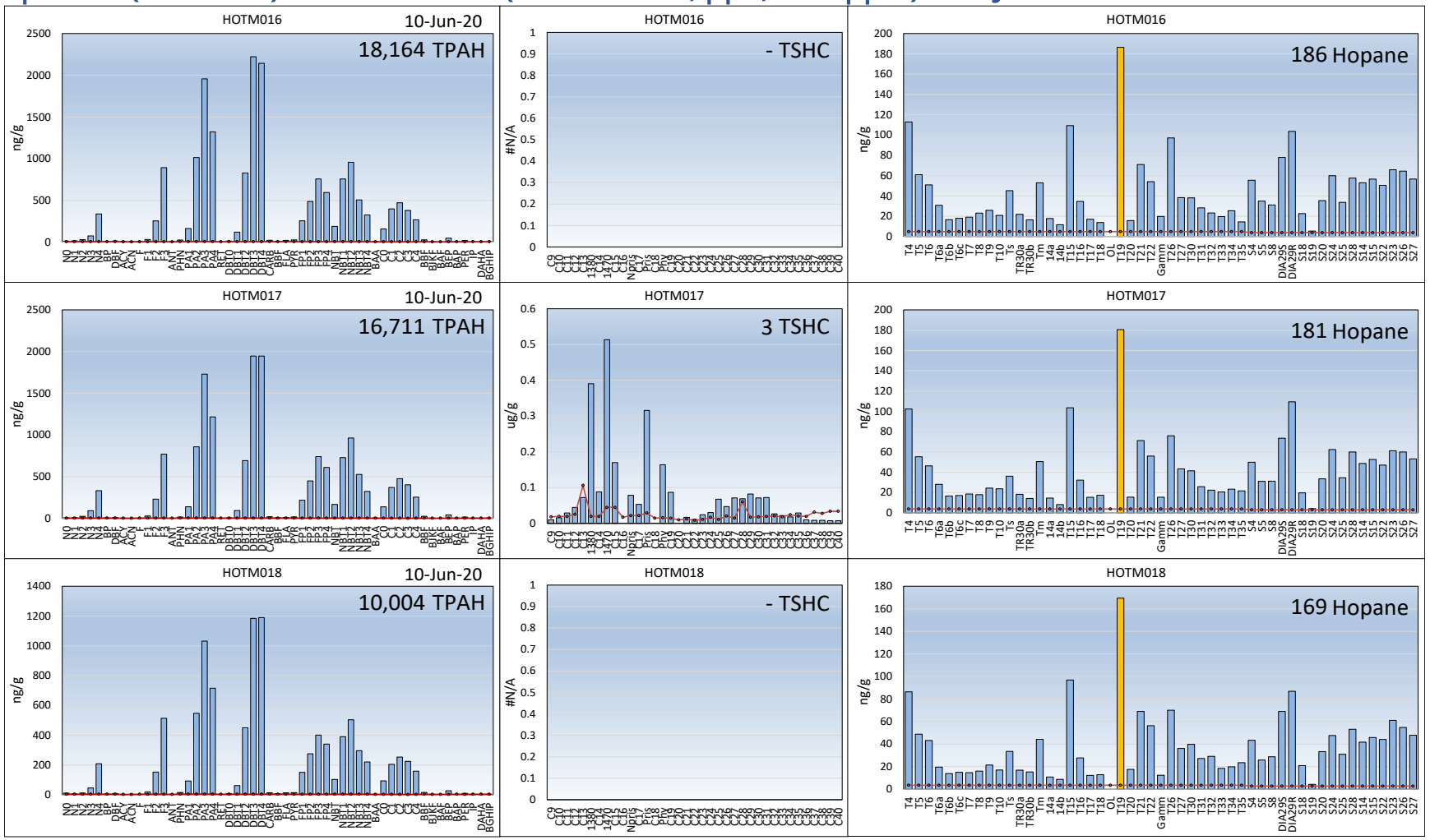

Spill site (Hot Zone) mussel tissues (PAH and S/T, ppb; SHC ppm) – 21 July

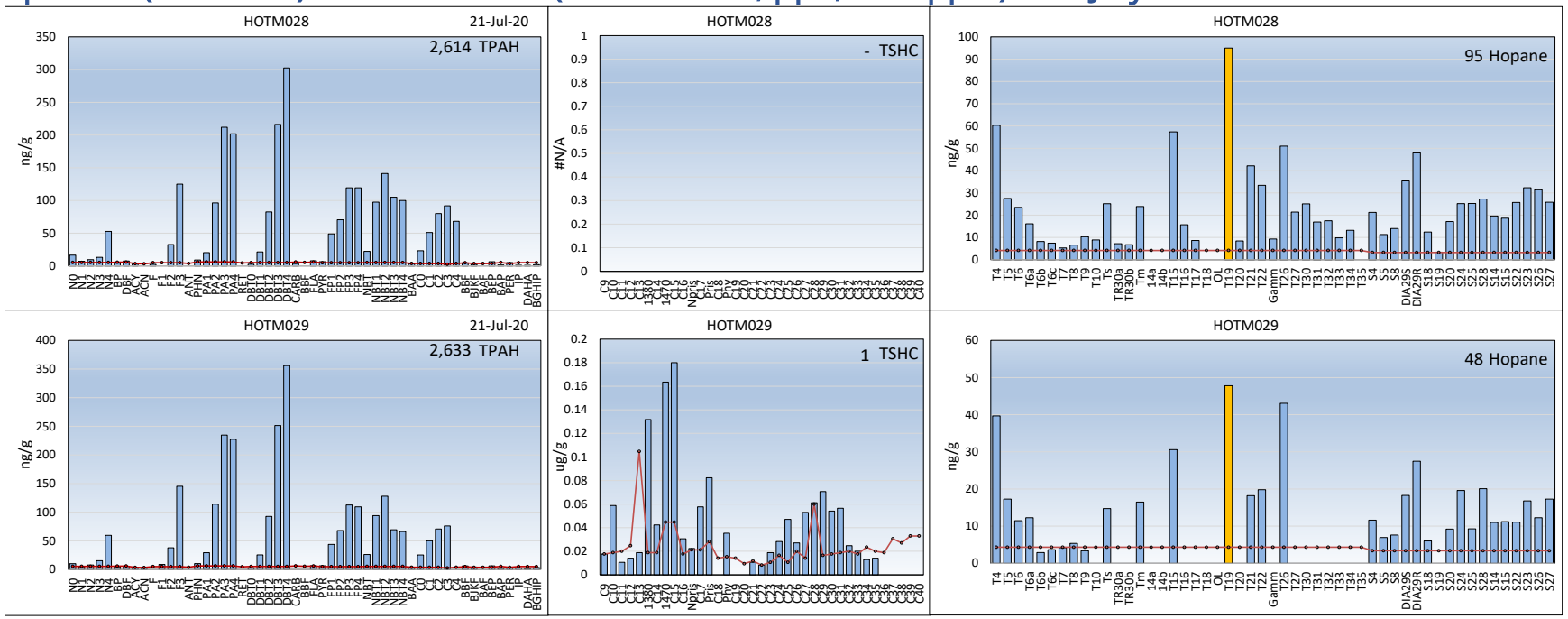

Jackson Point (JAP) (PAH and S/T, ppb; SHC ppm) -1 May

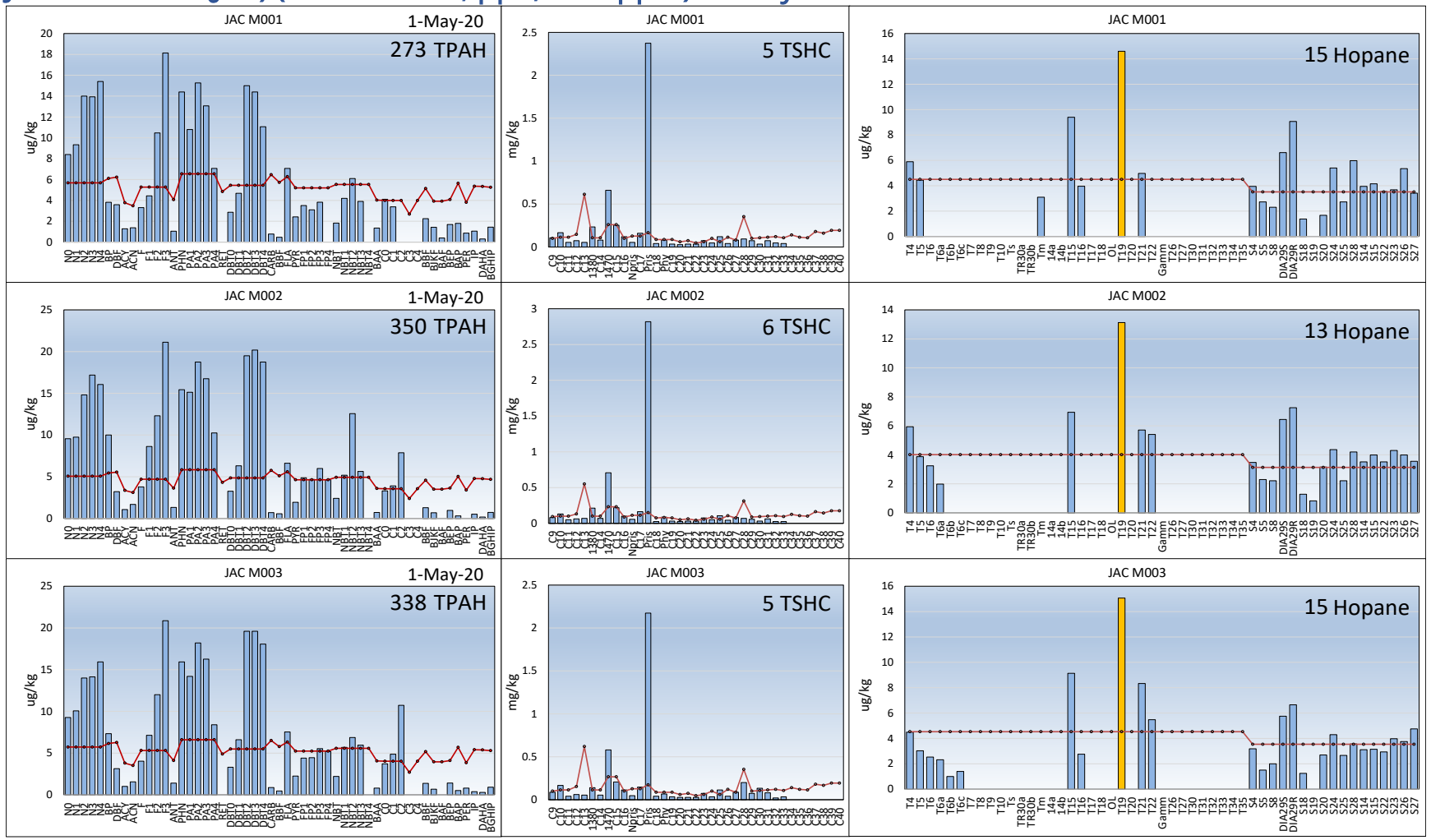

Jackson Point (JAP) (PAH and S/T, ppb; SHC ppm) -12 May

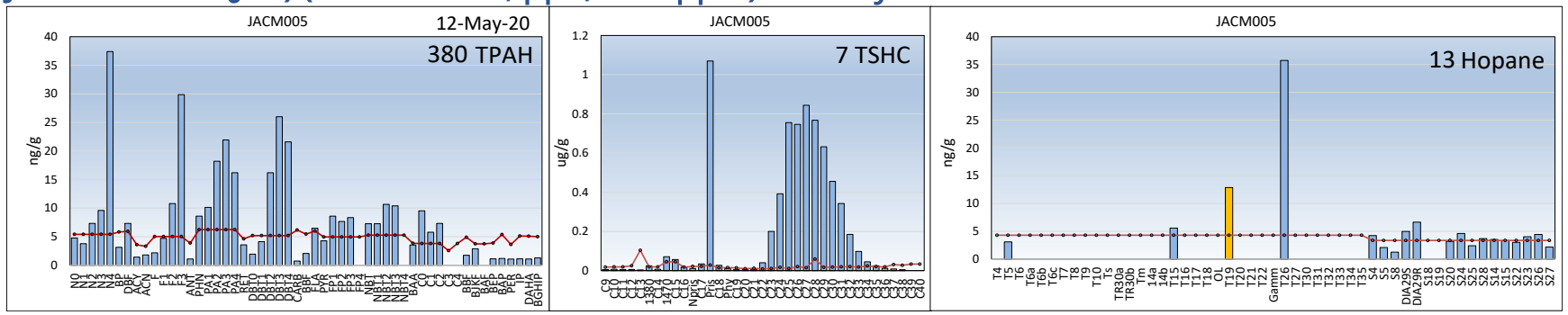

Jackson Point (JAP) (PAH and S/T, ppb; SHC ppm) -19 May

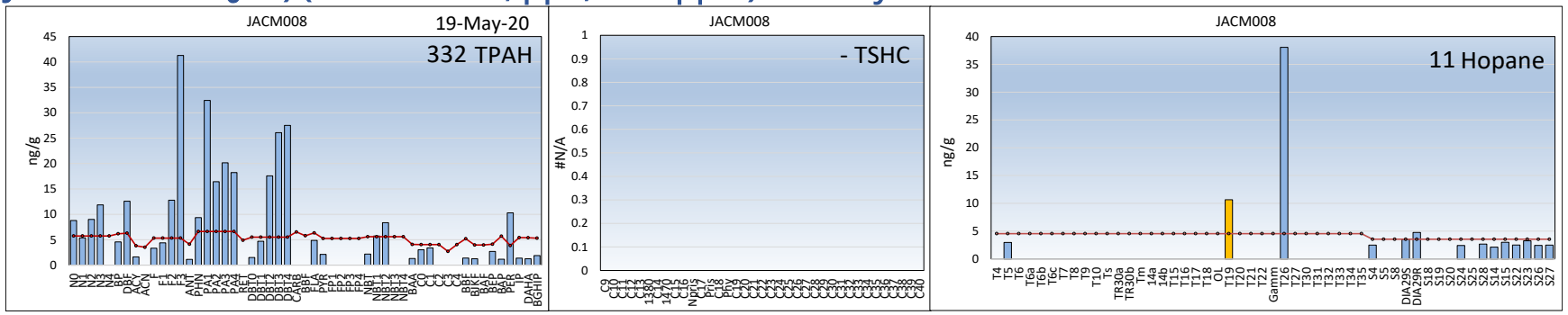

LTEMP Jackson Point (JAP) (PAH and S/T, ppb; SHC ppm) - 11 June

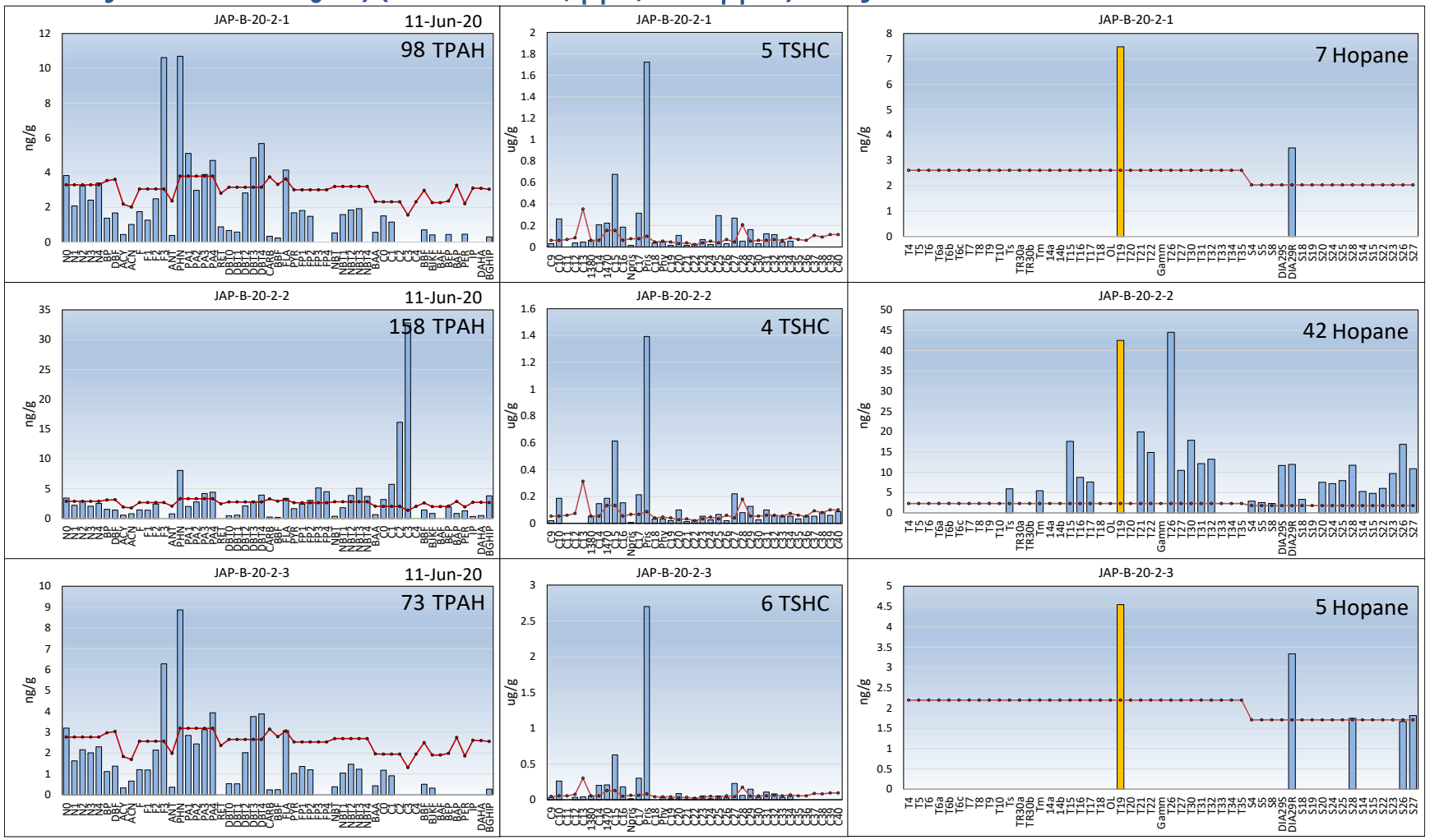

Jackson Point (JAP) (PAH and S/T, ppb; SHC ppm) - 22 July

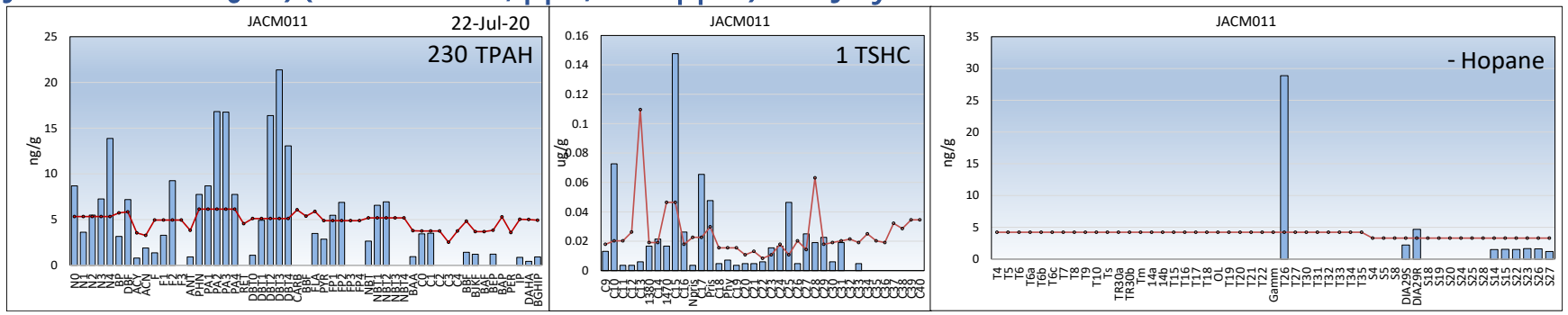

Saw Island (AMT) (PAH and S/T, ppb; SHC ppm) - 1 May

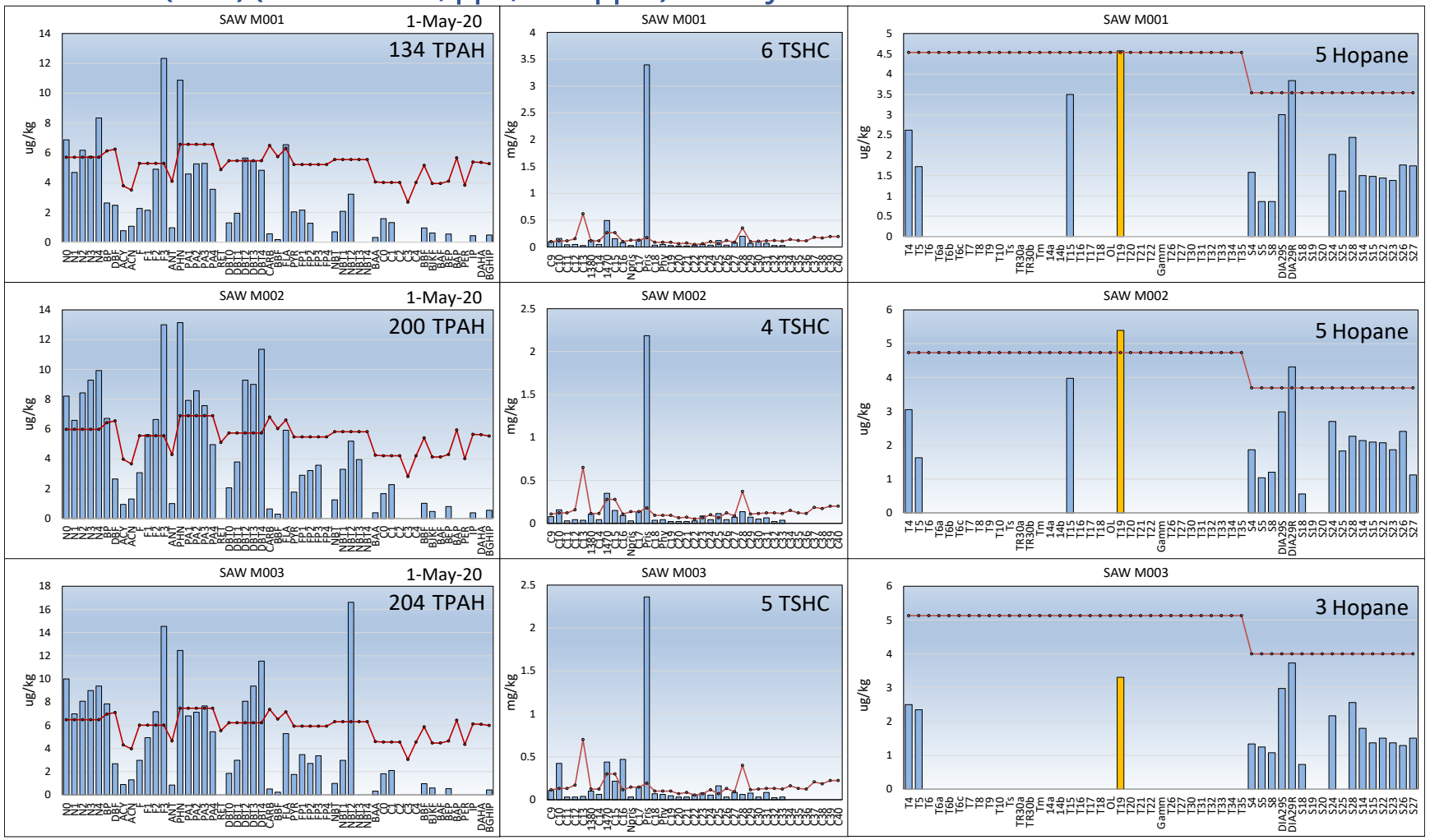

Saw Island (AMT) (PAH and S/T, ppb; SHC ppm) - 12 May

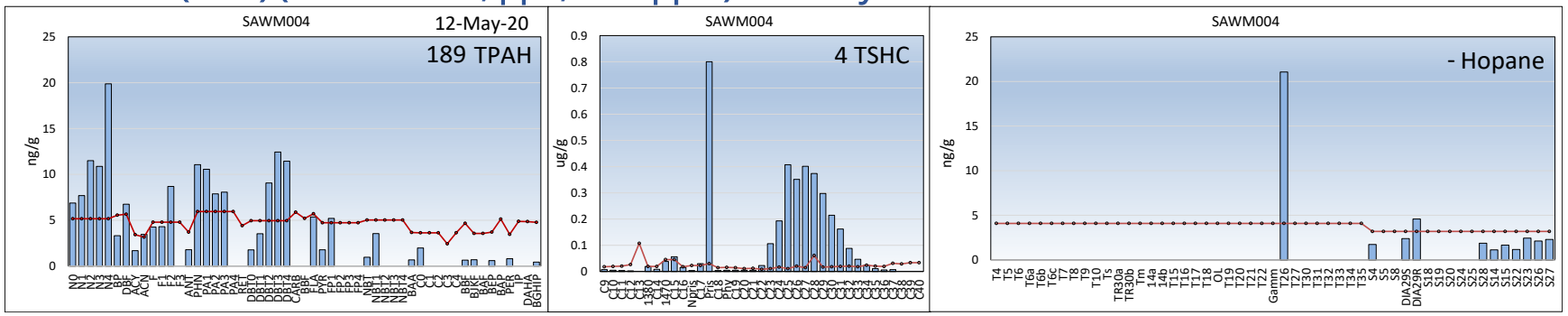

Saw Island (AMT) (PAH and S/T, ppb; SHC ppm) - 19 May

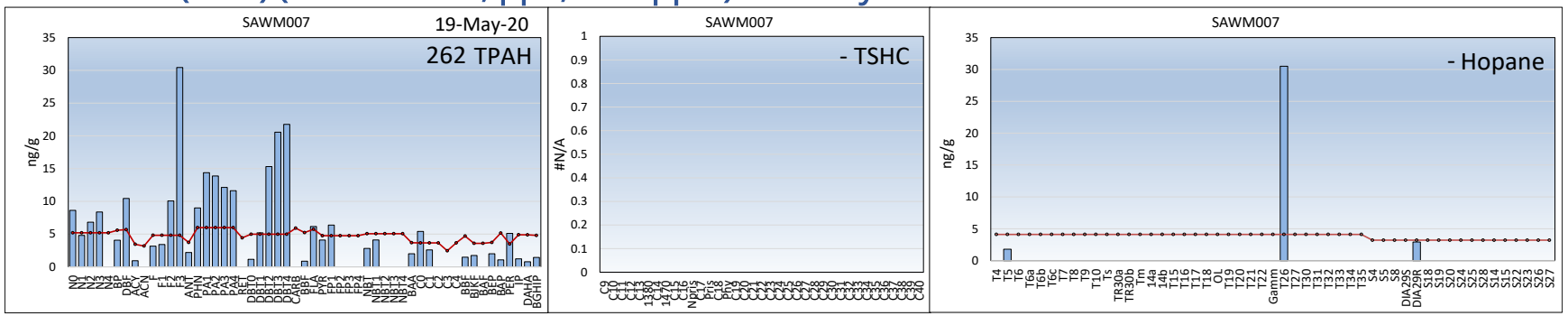

LTEMP Saw Island (AMT) (PAH and S/T, ppb; SHC ppm) - 11 June

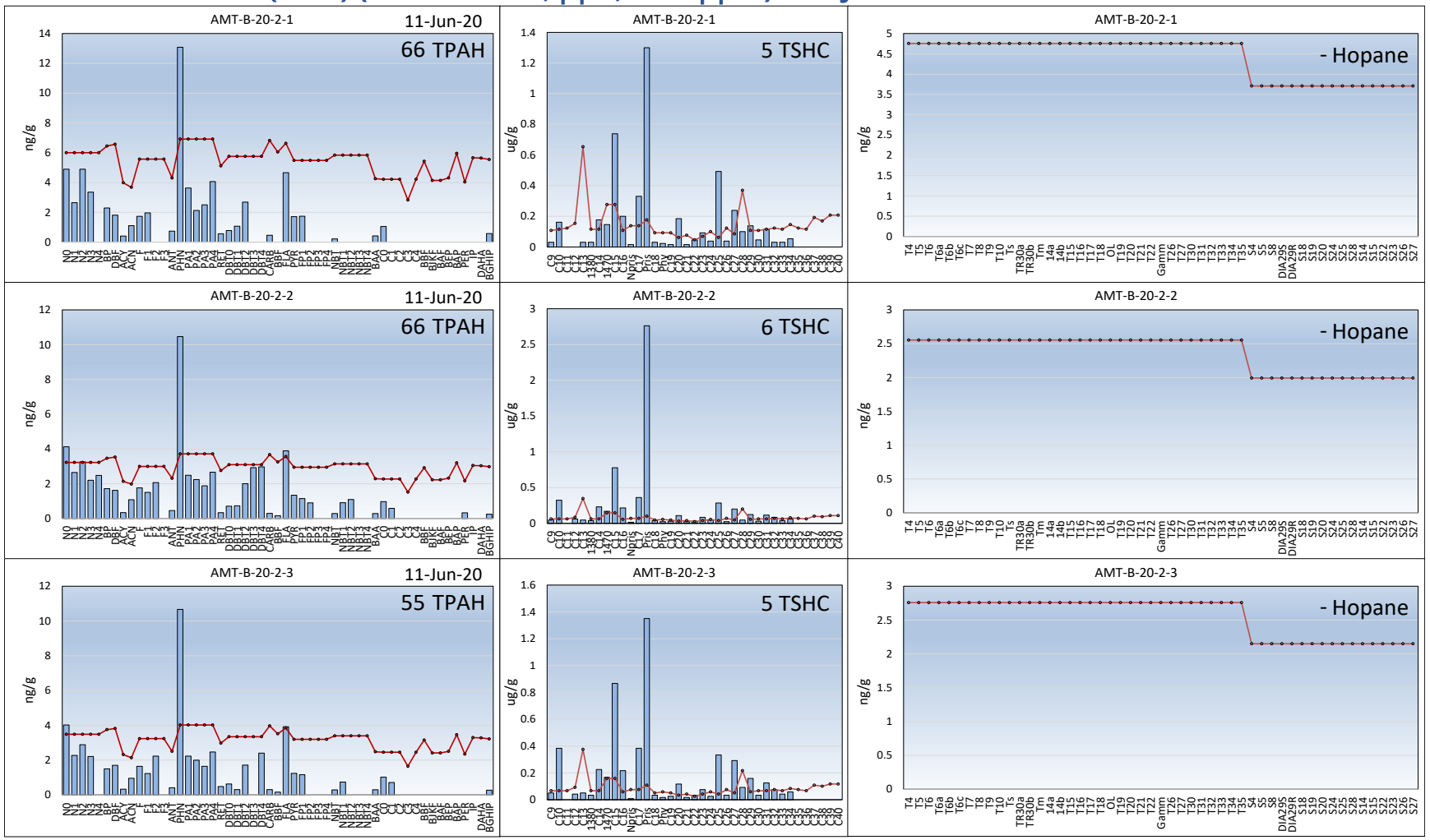

Saw Island (AMT) (PAH and S/T, ppb; SHC ppm) - 22 July

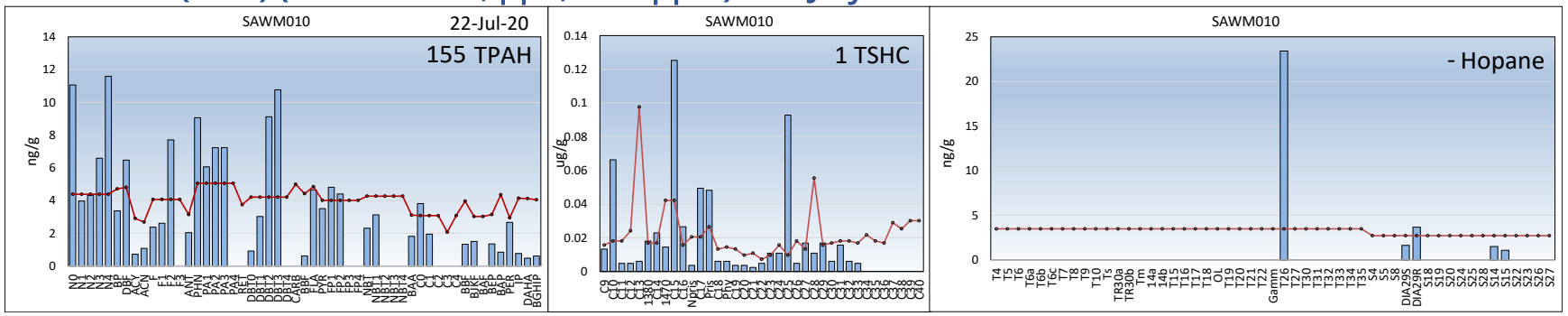

Jack Bay (PAH and S/T, ppb; SHC ppm) - 9 June

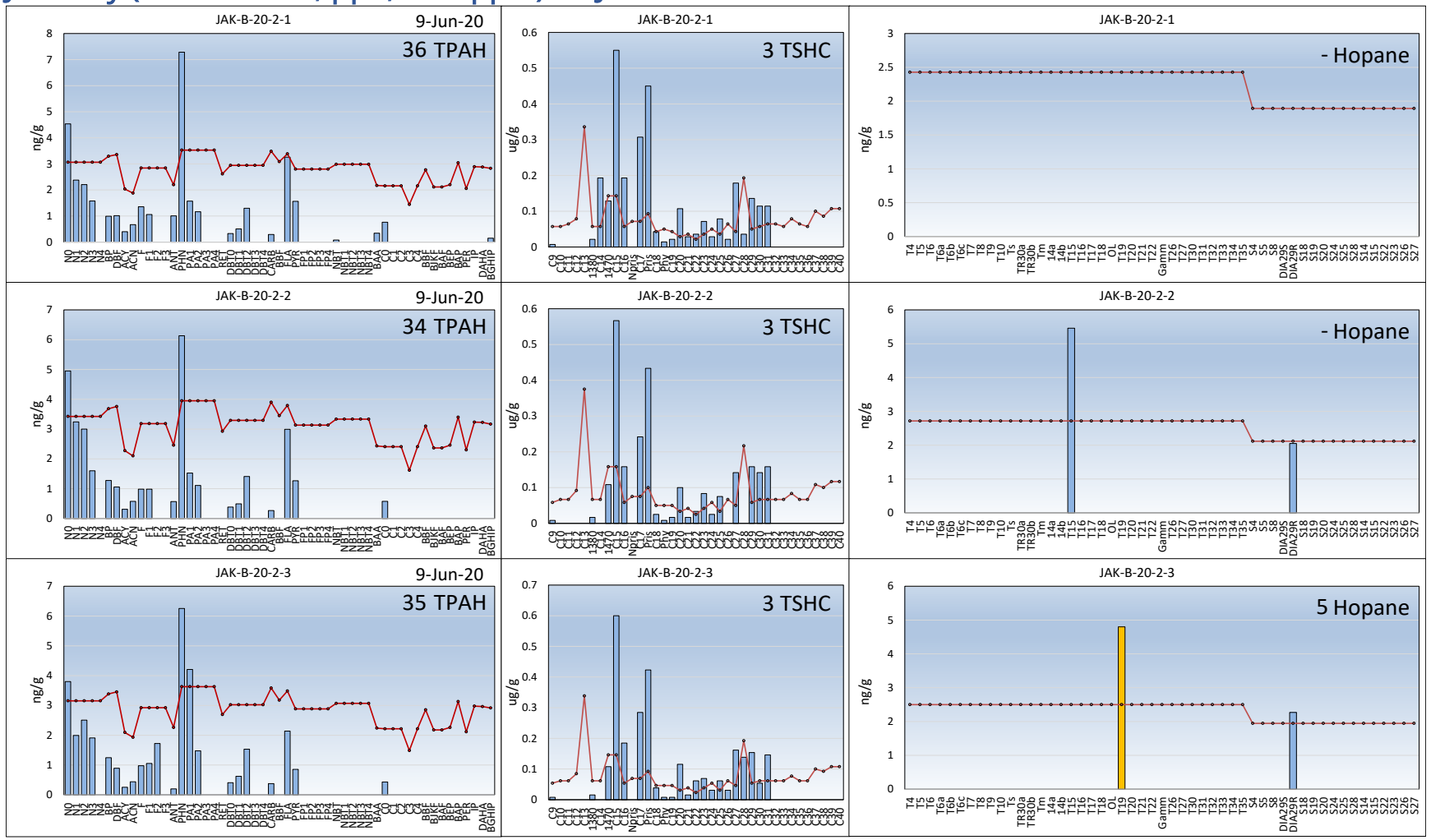

Galena Bay (PAH and S/T, ppb; SHC ppm) - 9 June

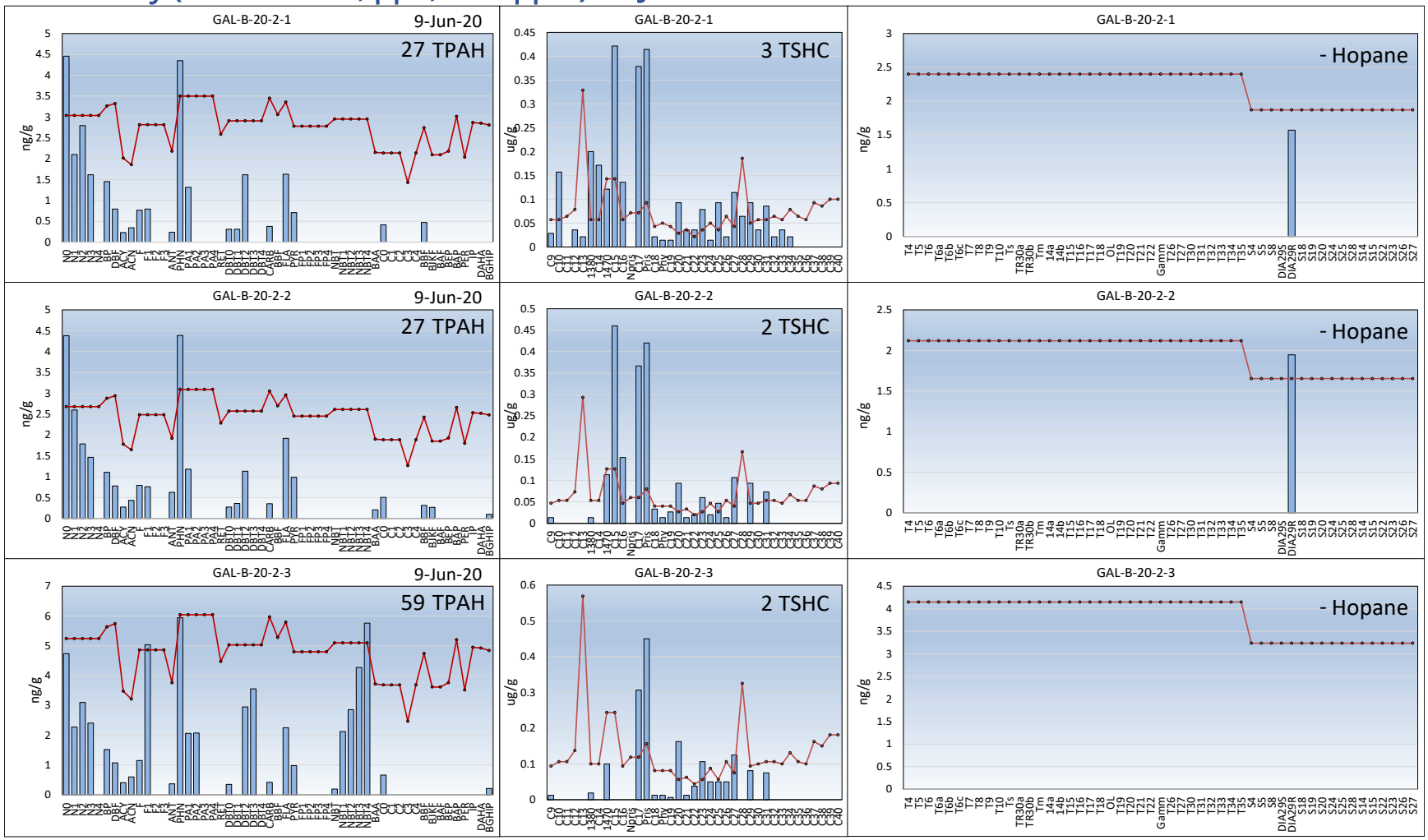

Appendix 4. Hydrocarbon Profiles

The following content details the samples' relevant hydrocarbon profile features in the reported time series and mussel samples from adjacent and remote locations (Fig. A4-1). They comprise three narratives: source, weathering, and spill management. The weathering reflects the natural process of evaporation, dissolution, photooxidation, and microbial degradation, all well documented processes. But spill management has affected sample concentrations. At the spill site, a series of containment booms were deployed to capture spreading slicks and protect the nearby islands (Fig. A4-2). One set of booms remained deployed around the spill origin as it continued to release the plume, and several were prudently kept in place until October. So, oil concentrations in the mussels were minimized at Saw Island and Jackson Point but maximized as chronic sheens were retained (and removed) at the spill site.

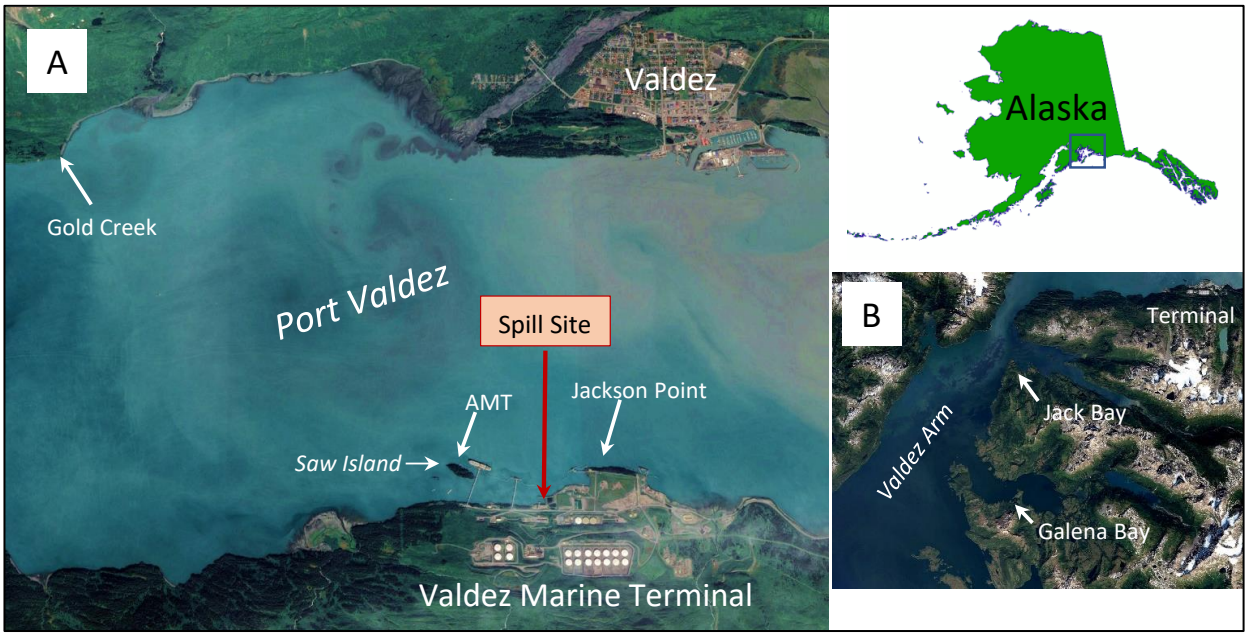

Fig. A4-1*. Overview of Port Valdez (A) showing the April 12, 2020, intertidal spill location at the Valdez Marine Terminal. Mussels were sampled at the Spill Site ("Hot Zone"), Jackson Point (JAP), Saw Island (AMT), and the control station at Gold Creek (GOC) 6 km to the northwest across the Port. Regional background samples were also collected at Jack Bay and Galena Bay (B) in June 2020.*

Fig. A4-2. Containment booms placed around the spill site and in adjacent waters. Saw Island in upper left background. Image from Alyeska Pipeline.

The spill source sample, collected from the shoreline on 30 April (Fig. A4-3), shows a freshly weathered ANS crude oil signature from the still seeping sump (Fig. A4-4). Missing are significant portions of the naphthalenes and lighter molecular weight n-alkanes below n-C_{15} that are typical of fresh ANS crude oil. Note the plotted concentration scales in the figure vary to facilitate profile comparisons. Oil concentrations for PAH, SHC, and S/T are in milligrams/kilogram (parts per million, ppm) whereas data for mussel tissues are presented in micrograms/kilogram dry wt. (parts per billion, ppb). This allows easy comparison of the PAH, SHC and S/T profiles, while total concentrations appear above the data in each plot.

Almost identical PAH, SHC, and S/T profiles are obtained comparing the source oil to the Day 1 spill site mussels (Fig. A4-4 top two profiles). Even slightly less weathered than the source oil sample, the initial tissue burdens appear with slightly greater relative contributions of lower-molecular-weight n-alkanes (n-C_{10} through n-C_{15}) compared to the higher molecular weight constituents. In comparing petroleum biomarker (S/T) profiles, mono- and tri-aromatic steroid constituents with molecular weights greater than the biomarker, ethylcholestane (S27) (see Appendix 2) are lost during the fractionation and lipid cleanup/removal process required for tissues. Therefore, biomarker constituent comparisons are limited to the triterpanes (T4) through ethylcholestane (S27).

Fig. A4-3*. Austin Love collecting the intertidal source-oil sample with a Teflon® net on April 30, 2020.*

From the adjacent Jackson Point station (Fig. A4-1), the PAH profiles from the Day 1 mussel collections show three orders of magnitude lower concentrations, and the n-alkanes showed none of the evenly repeating odd- and even-carbon number series from n-C_{12} through n-C_{40} observed in the spill oil or at the spill site (Fig. A4-4, top two panels). Instead, at both Jackson Point and Saw Island the SHC fractions are characterized by dominant marine biogenic isoprenoids, trimethyltridecane (1470) and pristane (Blumer et al., 1963; Blumer et al., 1971; NRC, 1985). While most of the PAH at Jackson Point are above the method detection limit (MDL, red line), many PAH at Saw Island are below the MDL. These data indicate that although some of the spilled oil did reach Jackson Point, most of the oil was contained within the booms laid out in response to the spill (Fig. 2 and Fig. A4-2). Background PAH and SHC profiles from Jackson Point mussels collected in the previous year, 2019, allow a dramatic pre- and post-oiling comparison at this station (Fig. A4-5). The samples' PAH on July 22 (Day 83) document that oil still persisted although, lacking sufficient biomarkers, it cannot be positively attributed to the spill.

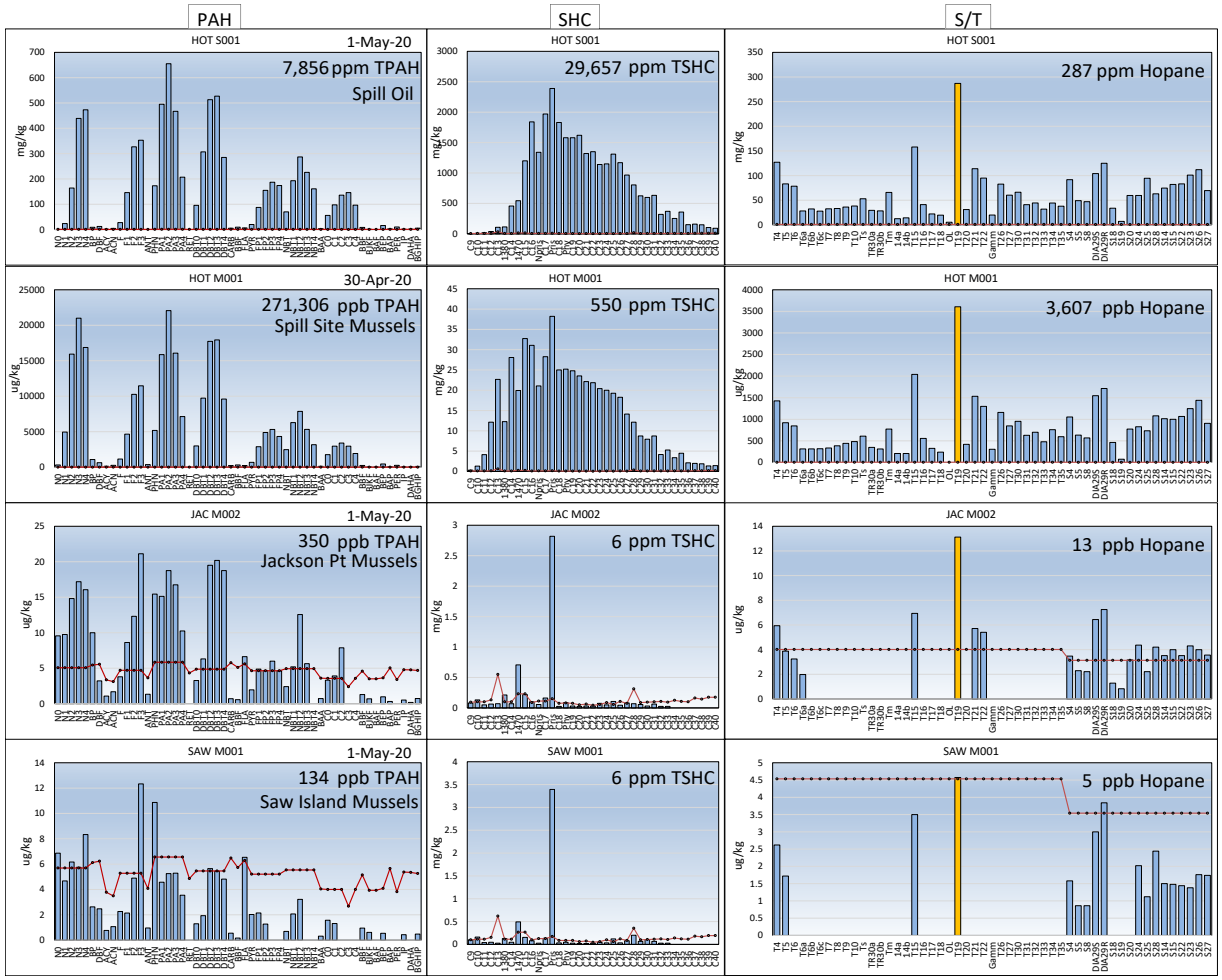

Fig. A4-4*. Initial PAH, SHC, and petroleum biomarker (S/T) profiles of spill oil and mussels collected on Day 1-2 from the Spill Site, Jackson Point (JAP), and Saw Island (AMT). Note the concentration units change in scaling oil vs tissue matrices; ppm for oil and SHC, ppb for tissues PAH and S/T. Red line is the sample-specific method detection limit (MDL).*

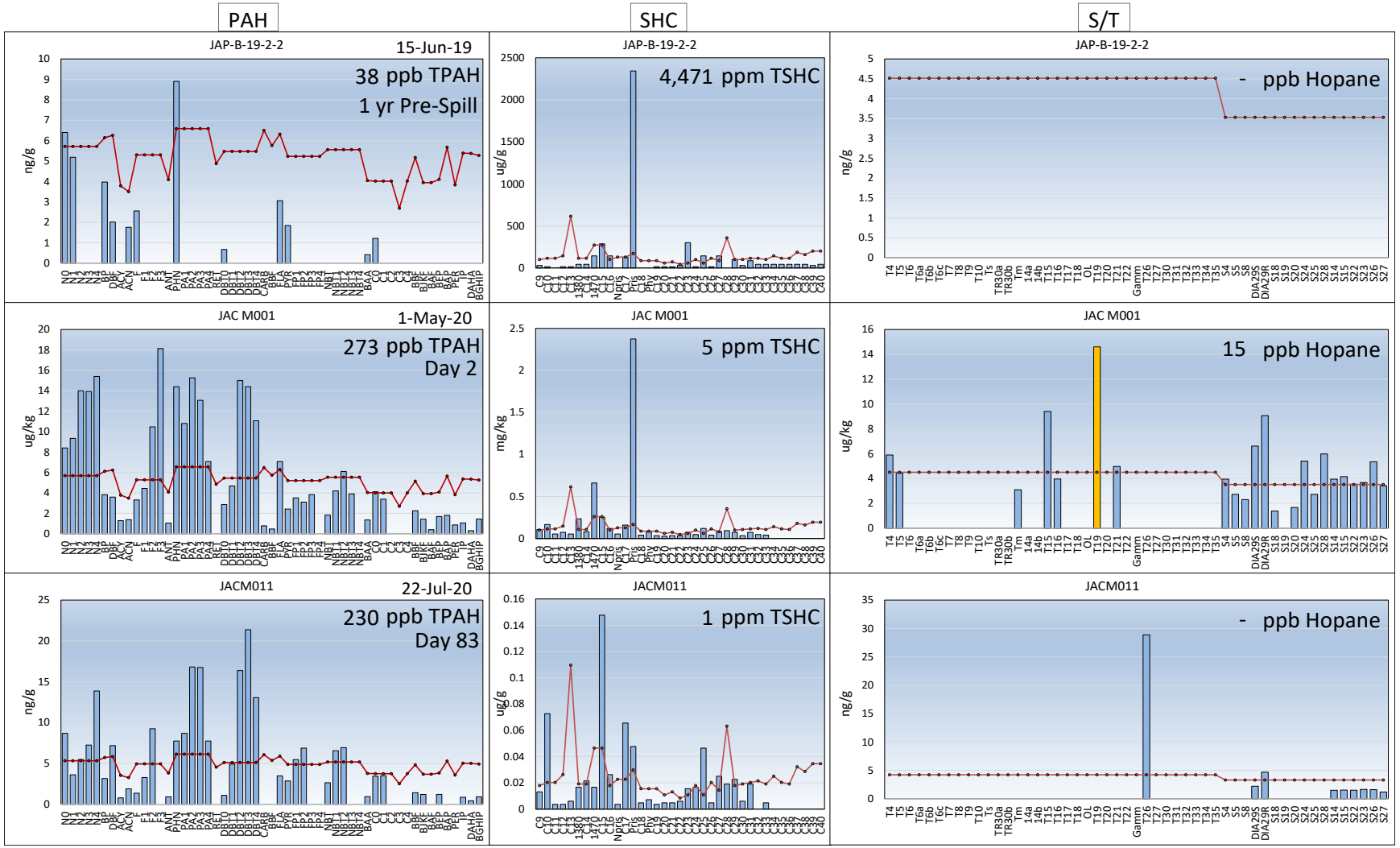

Fig. A4-5*. Jackson Point mussels pre-spill (2019), Day 2 (18 days post spill) and Day 83 of the study. Red line is the sample specific method detection limit (MDL).*

From mussel collected as part of the normal LTEMP monitoring activities in June 2020 (study days 42-44), the profiles suggested that the adjacent traditional stations at JAP and AMT had largely returned to pre-spill conditions with most of the PAH at or below the sample-specific MDLs (Fig. A4-6). The PAH that were detected were largely parent-dominated, combustion products (e.g., phenanthrene (PHN) > C1-PHN) (Farrington et al., 1982). The SHC fractions at these stations were primarily marine biogenic hydrocarbons, n-C_{15}, n-C_{17}, and pristane along with traces of odd-carbon-numbered n-C_{23} to n-C_{31} from terrestrial plant waxes (NRC, 1985). The petroleum biomarker (S/T) profiles at the LTEMP stations showed no evidence of lingering oil from the April 12th spill. At the spill site (top profiles in Fig. A4-6), however, the data depict significant lingering oil in the mussels in June 2020 (study day 42), and with the petroleum biomarker profiles, it is easily traced back to the April 12th sump overflow.

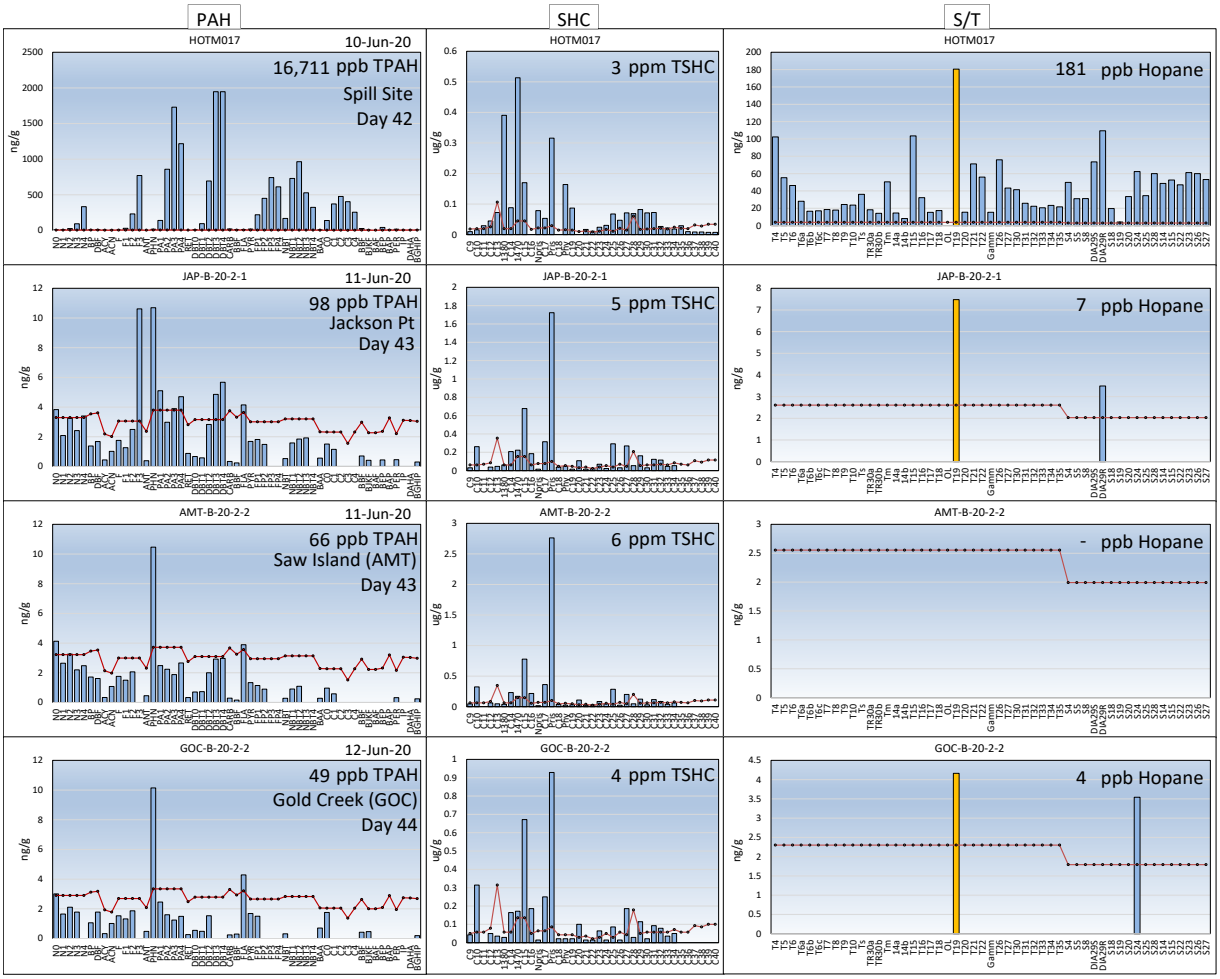

Fig. A4-6*. Port Valdez LTEMP tissue results showing June 2020 recovery (Day 41-44) with high residual spill-hydrocarbons remaining at the Spill Site and near- or below-MDL, mixed pyrogenic-dominated PAH patterns and biogenic SHC at JAP, AMT, and GOC. Red line is the sample specific method detection limit (MDL).*

Non-exposed mussels for gene transcription and chemistry controls were also collected from remote locations (Jack Bay and Galena Bay) within the Port Valdez fjord in June 2020 (Fig. A4-1). They showed primarily parent, non-alkylated combustion products with below MDL traces of alkylated homologues in the PAH profiles, traces of marine biogenic isoprenoids (1470 and pristane), n-C_{17}, and odd-carbon-number dominated n-C_{23} to n-C_{31} plant waxes derived from terrestrial vegetation (NRC, 1985). No hopane was observed in any or the remote-site samples (Fig. A4-7).

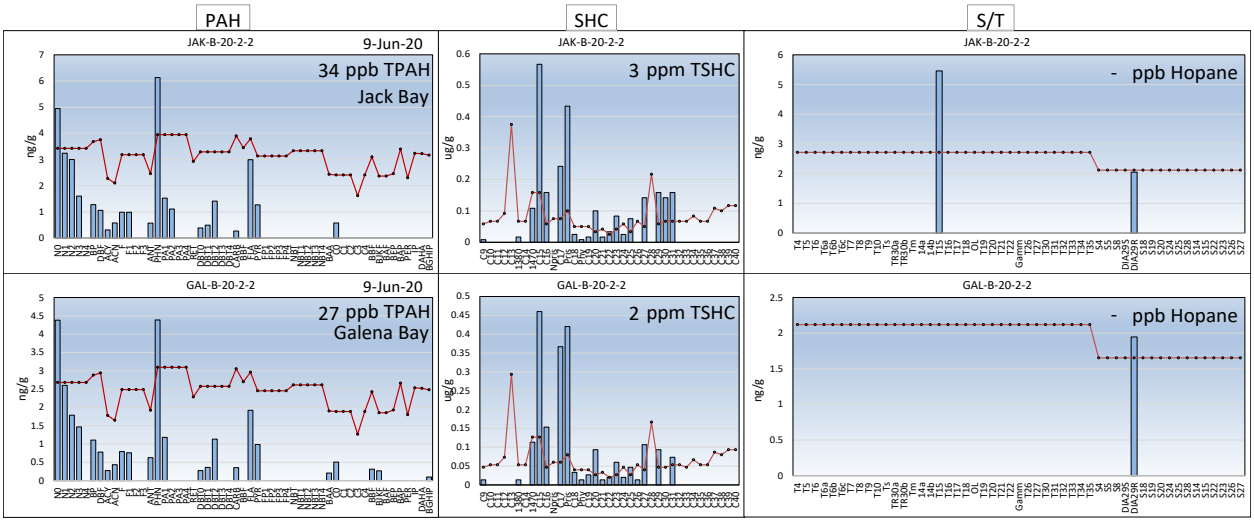

Fig. A4-7*. PAH, SHC, and S/T profiles from mussels at the remote sites, Jack Bay and Galena Bay. The profiles show only traces of above-MDL combustion products and biogenic marine and terrestrial SHC. The red line is the sample-specific method detection limit.*

Weathering of the spill site mussel PAH profiles is seen by the time series loss of the more water-soluble parent- and lower-alkylated PAH within each homologous group (Fig. A4-8). The red line superimposed over the PAH and S/T profiles represents the pattern expected from the source oil (normalized to C2-chrysene measured in each sample). The SHC are normalized against the measured n-C_{32}. The S/T overlay is the expected S/T profile from the Day 1 sample normalized against the measured hopane. Significant quantities of the spill oil remain in the spill site samples through study Day 83 (July 21, 100 days from the initial spill). These data were used for retention half-life calculations and are further discussed in the depuration section (Appendix 5).

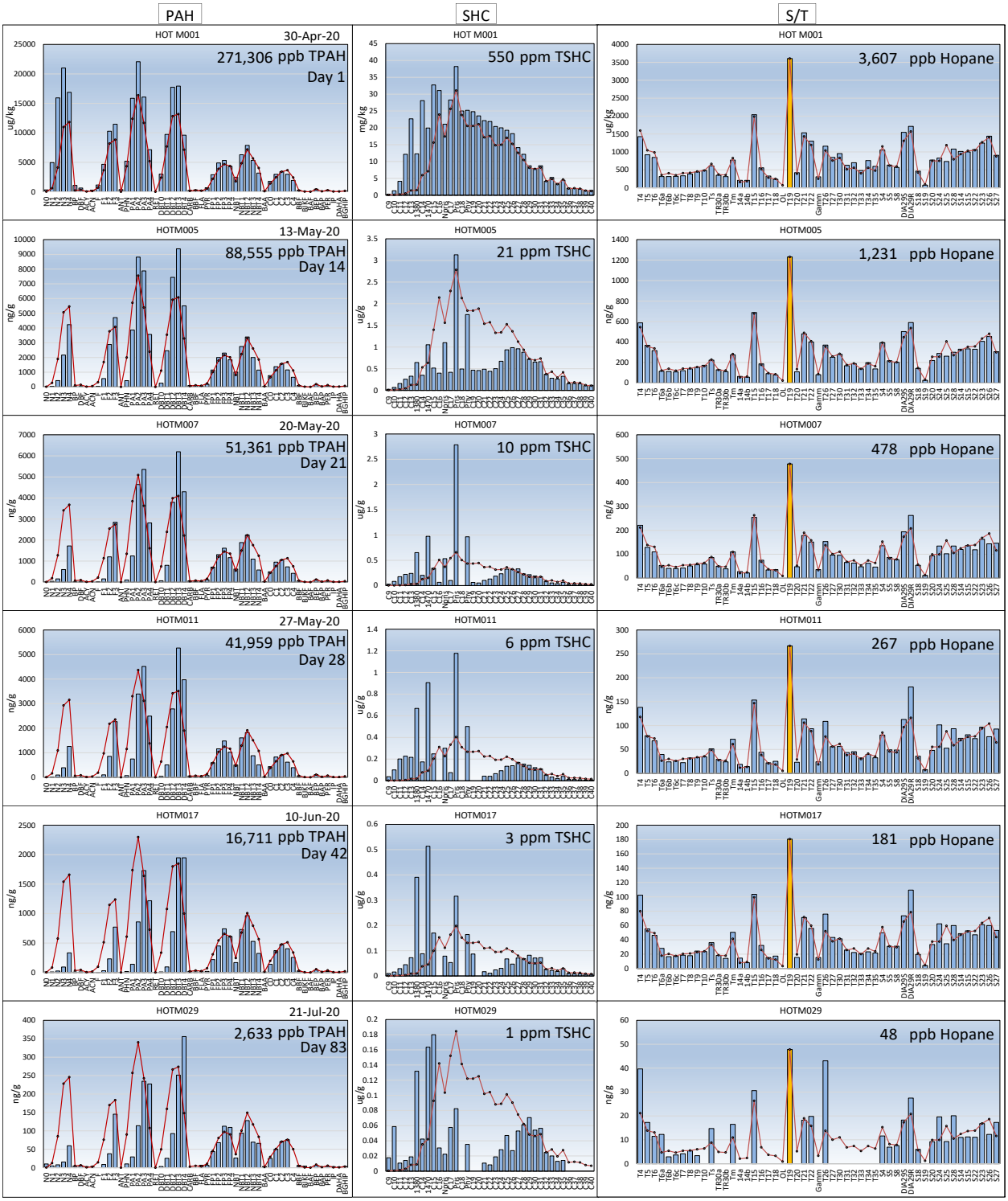

Fig. A4-8*. PAH, SHC, and S/T profiles of Spill Site (Hot Zone) mussels (ppb) showing the weathering trends over time. Red lines denote the Day 1 oil profile with its PAH scaled to each sample's C-2 chrysene, SHC to n-C_{32}, and S/T to hopane.*

Appendix 5. Tissue Depuration

As mentioned in the paper, viewed by their homologous groupings (Fig. A5-1), depuration rates slowed with increasing alkylation (parent, C1-, C2-, C3-, C4- homologs) and increasing molecular weight (left column then right column). Accumulation patterns first appear in C4-phenanthrene. Decalins, a non-aromatic cyclic compound (not a PAH), are accumulating from an unknown secondary source (top left panel).

Viewed by log K_{OW} values (Table A5-1), the patterns just described appear related to log K_{OW} values. Sorted by homologous families, note the log K_{OW} values increase with alkylation (left columns). Sorted by log K_{OW} (right columns), the spark-line plots appear as unit-less, sequential (not time-scaled) trend lines. Note that accumulating (increasing) trends do not appear before log K_{OW} ~6.3. Uniquely anomalous are several PAH, like acenaphthene, fluoranthene, C3-fluoranthene/pyrene and benzo[b]fluoranthene with a non-trending, concentration bump midway through the time series. The source of the patterns is uncertain. Also, several of the trend lines have an uptick to end the time series. These are considered lab artifacts (flagged as estimated values) whereby detection was confirmed but below quantitation limits. Also, several analytes flat-line as non-detects. Yet behind this noisy data, log K_{OW}-related depuration trends are apparent.

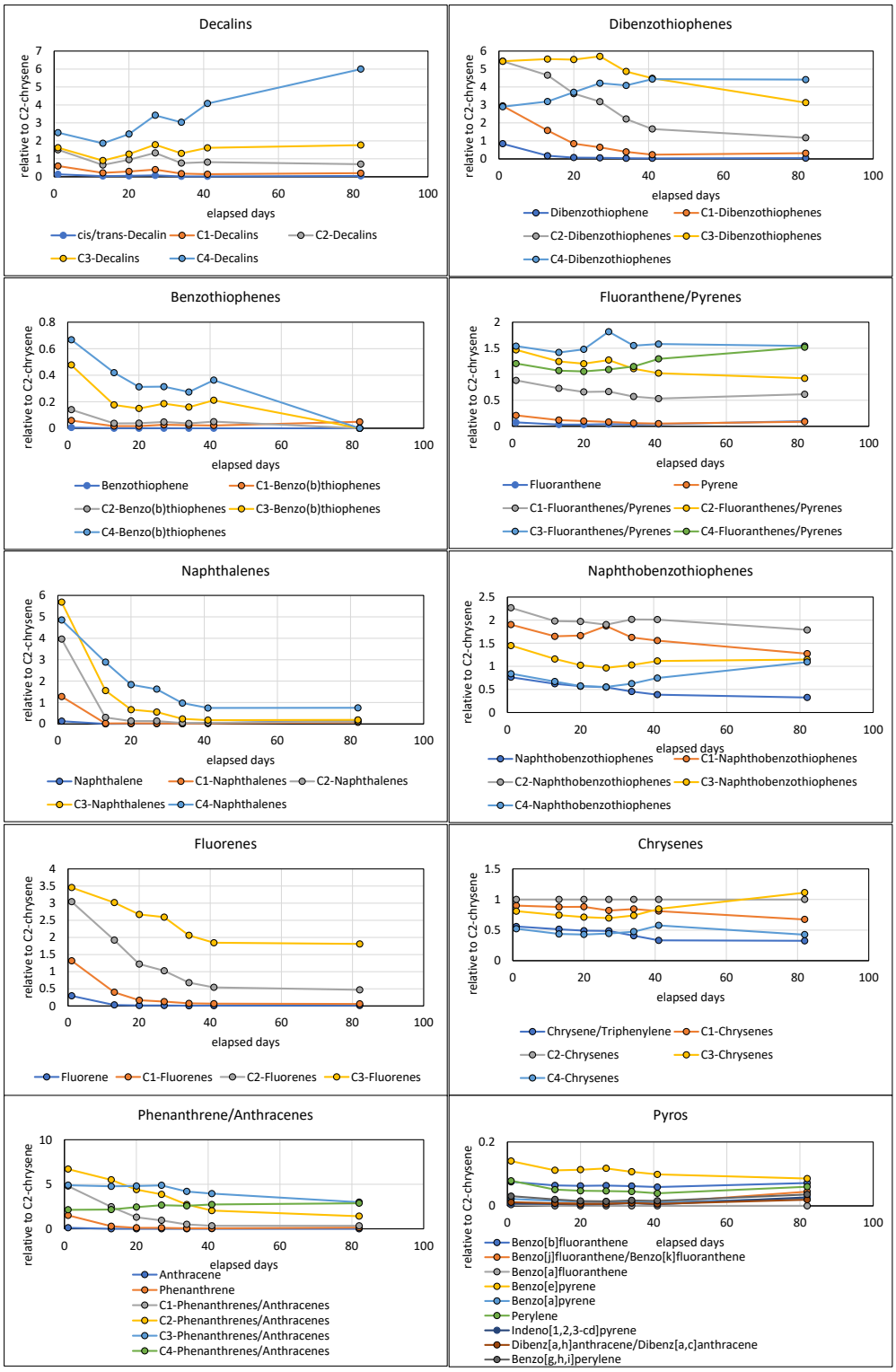

Fig. A5-1*. Time series of proportional concentrations of PAH families (relative to C2-chrysene for visual discrimination) in spill site (Hot Zone) mussels. Most show simple log decay depletion curves but others show accumulation (e.g., C4-phenanthrene/anthracene) or a mixed response (e.g., C1-, C2- and C3-naphthobenzothiophene).*

Table A5-1. PAH analytes and depuration trends sorted by homologous families (in GC elution order) (left columns) and by solubility, log K_{OW} (right columns). Lipophilicity, log K_{LIPW}, is calculated from log K_{OW}. Depuration curves based on C2-chrysene normalized values, depict a modality of simple depletion vs accumulation. Here, the trend lines are unit-less and just sequential, not time-scaled. PAH ordered by log K_{OW} (right columns) show a general transition from simple depletion to accumulation or mixed response when log K_{OW} value > 6.3 (grey highlighted K_{OW} values). Singular upticks at the end of trend lines are trace-level lab artifacts.

PAH by homologus families	log Kow	log Klipw	Depuration
Benzo(b)thiophene	3.12	3.12	
C1-Benzo(b)thiopenes	3.65	3.72	
C2-Benzo(b)thiophenes	4.17	4.31	
C3-Benzo(b)thiopenes	4.66	4.87	
C4-Benzo(b)thiopenes	5.18	5.46	
Naphthalene	3.37	3.40	
C1-Naphthalenes	3.87	3.97	
C2-Naphthalenes	4.38	4.55	
C3-Naphthalenes	5.00	5.26	
C4-Naphthalenes	5.30	5.60	
Acenaphthene	3.92	4.03	
Acenaphthylene	4.00	4.12	
Fluorene	4.18	4.32	
C1-Fluorenes	4.97	5.22	
C2-Fluorenes	5.20	5.48	
C3-Fluorenes	5.70	6.05	
Anthracene	4.54	4.73	
Phenanthrene	4.57	4.77	
C1-Phenanthrenes/anthracenes	5.12	5.39	
C2-Phenanthrenes/anthracenes	5.25	5.54	
C3-Phenanthrenes/anthracenes	5.92	6.30	
C4-Phenanthrenes/anthracenes	6.32	6.76	
Dibenzothiophene	4.34	4.51	
C1-Dibenzothiophenes	4.86	5.10	
C2-Dibenzothiophenes	5.33	5.63	
C3-Dibenzothiophenes	5.81	6.18	
C4-Dibenzothiophenes	6.34	6.78	
Benzo(b)fluorene	5.75	6.11	
Fluoranthene	5.22	5.51	
Pyrene	5.18	5.46	
C1-Fluoranthenes/pyrenes	5.29	5.59	
C2-Fluoranthenes/pyrenes	5.56	5.89	
C3-Fluoranthenes/pyrenes	6.28	6.71	
C4-Fluoranthenes/pyrenes	6.69	7.18	
Naphthobenzothiophene	5.60	5.94	
C1-Naphthobenzothiophenes	6.38	6.82	
C2-Naphthobenzothiophenes	6.87	7.38	
C3-Naphthobenzothiophenes	7.37	7.95	
C4-Naphthobenzothiophenes	7.79	8.43	
Benzo(a)anthracene	5.91	6.29	
Chrysene + Triphenylene	5.55	5.88	
Chrysene	5.86	6.23	
C1-Chrysenes	6.14	6.55	
C2-Chrysenes	6.59	7.06	
C3-Chrysenes	6.97	7.50	
C4-Chrysenes	7.42	8.01	
Benzo(b)fluoranthene	5.80	6.17	
Benzo(j+k)fluoranthene	6.20	6.62	
Benzo(a)fluoranthene	6.54	7.01	
Benzo(e)pyrene	6.44	6.89	
Benzo(a)pyrene	6.35	6.79	
Perylene	6.25	6.68	
Indeno(1,2,3-c,d)pyrene	7.53	8.13	
Dibenz(a,h+a,c)anthracene	6.75	7.25	
Benzo(g,h,i)perylene	6.50	6.96	

PAH by log Kow	log Kow	log Klipw	Depuration
Benzo(b)thiophene	3.12	3.12	
Naphthalene	3.37	3.40	
C1-Benzo(b)thiophenes	3.65	3.72	
C1-Naphthalenes	3.87	3.97	
Acenaphthene	3.92	4.03	
Acenaphthylene	4.00	4.12	
C2-Benzo(b)thiophenes	4.17	4.31	
Fluorene	4.18	4.32	
Dibenzothiophene	4.34	4.51	
C2-Naphthalenes	4.38	4.55	
Anthracene	4.54	4.73	
Phenanthrene	4.57	4.77	
C3-Benzo(b)thiophenes	4.66	4.87	
C1-Dibenzothiophenes	4.86	5.10	
C1-Fluorenes	4.97	5.22	
C3-Naphthalenes	5.00	5.26	
C1-Phenanthrenes/anthracenes	5.12	5.39	
C4-Benzo(b)thiophenes	5.18	5.46	
Pyrene	5.18	5.46	
C2-Fluorenes	5.20	5.48	
Fluoranthene	5.22	5.51	
C2-Phenanthrenes/anthracenes	5.25	5.54	
C1-Fluoranthenes/pyrenes	5.29	5.59	
C4-Naphthalenes	5.30	5.60	
C2-Dibenzothiophenes	5.33	5.63	
Chrysene + Triphenylene	5.55	5.88	
C2-Fluoranthenes/pyrenes	5.56	5.89	
Naphthobenzothiophene	5.60	5.94	
C3-Fluorenes	5.70	6.05	
Benzo(b)fluorene	5.75	6.11	
Benzo(b)fluoranthene	5.80	6.17	
C3-Dibenzothiophenes	5.81	6.18	
Chrysene	5.86	6.23	
Benzo(a)anthracene	5.91	6.29	
C3-Phenanthrenes/anthracenes	5.92	6.30	
C1-Chrysenes	6.14	6.55	
Benzo(j+k)fluoranthene	6.20	6.62	
Perylene	6.25	6.68	
C3-Fluoranthenes/pyrenes	6.28	6.71	
C4-Phenanthrenes/anthracenes	6.32	6.76	
C4-Dibenzothiophenes	6.34	6.78	
Benzo(a)pyrene	6.35	6.79	
C1-Naphthobenzothiophenes	6.38	6.82	
Benzo(e)pyrene	6.44	6.89	
Benzo(g,h,i)perylene	6.50	6.96	
Benzo(a)fluoranthene	6.54	7.01	
C2-Chrysenes	6.59	7.06	
C4-Fluoranthenes/pyrenes	6.69	7.18	
Dibenz(a,h+a,c)anthracene	6.75	7.25	
C2-Naphthobenzothiophenes	6.87	7.38	
C3-Chrysenes	6.97	7.50	
C3-Naphthobenzothiophenes	7.37	7.95	
C4-Chrysenes	7.42	8.01	
Indeno(1,2,3-c,d)pyrene	7.53	8.13	
C4-Naphthobenzothiophenes	7.79	8.43	

These log K_{OW} transition patterns may suggest why some PAH would simply deplete while others accumulate. Early studies proposed a "multiple compartment model" whereby some of the accumulated hydrocarbons are released rapidly before a much slower release of those remaining (Stegeman and Teal, 1973; Farrington et al., 1982; Mason, 1988). They report that chronically polluted bivalves lose their burden more slowly because the hydrocarbons have been accumulated into "stable compartments" that are not available

for rapid depuration. Mason proposed that after 46 days, the depuration curve of 0.15 ppm oil exposure could be broken into two exponential rate losses: "fast" during the first 28 days and "slower" thereafter. Two depuration rates support a concept of gut clearance of an accumulated substance followed by slower tissue clearance, the latter either diffusively or being metabolized via the mussel's AHR detox system.

Lipophilicity (lipid affinity) is a molecule's key property in transport processes, including intestinal absorption, membrane permeability, protein binding, and distribution to different tissues and organs. Endo et al. (2011) address this affinity mechanism in tissues by modeling differences in accumulation properties of neutral organic molecules (including PAH) between different types of lipids, i.e., accumulation into storage lipids versus membrane lipids. They find that a molecule's lipid affinity, expressed as log K_{LIPW} (liposome/water partitioning coefficient, the inverse to water solubility) reasonably correlates to log K_{OW} (octanol/water partitioning coefficient) but suggests that polyparameter linear free energy relationships (PP-LLFERs) are more concise. Note that accumulation may also result from PAH interactions with non-lipids such as proteins, however, lipid storage models match well with organism results (Endo et al., 2011).

These lipophilicity concepts work well for the traditional suite of PAH but not so much for polar or extreme hydrophobic compounds, including the entire suite of petroleum (S/T) biomarkers. For example, the recalcitrant forensic tracer, 17β(H),21β(H)-hopane, is mostly insoluble in water with high log K_{OW} values (estimated to be in the 10-15 range depending on the modeling program vs 3-7 for traditional PAH). From its depletion plot in mussel tissue (Fig. 4) hopane shows a simple logarithmic depletion trend and demonstrates no sign of accumulation despite its log K_{OW} implying it to be highly lipophilic. The same is true for all the reported petroleum biomarkers; triterpenes, hopanes and steranes show only simple depletion trends (n=13, 20, 17 analytes respectively) (Fig. A5-2) with only a couple of exceptions in the results section.

A mechanistic/free energy lipid-storage paradigm (Endo et al., 2011) suggests a reason for their lipophobic behavior. Hopanes as a group are non-aromatic C30 pentacyclic triterpanes (i.e., composed of six isoprene subunits) consisting of four six-membered rings and one five-membered ring (Fig. A5-3). Commonly containing 27-35 carbon atoms, they derive from precursors in bacterial bi-lipid membranes.

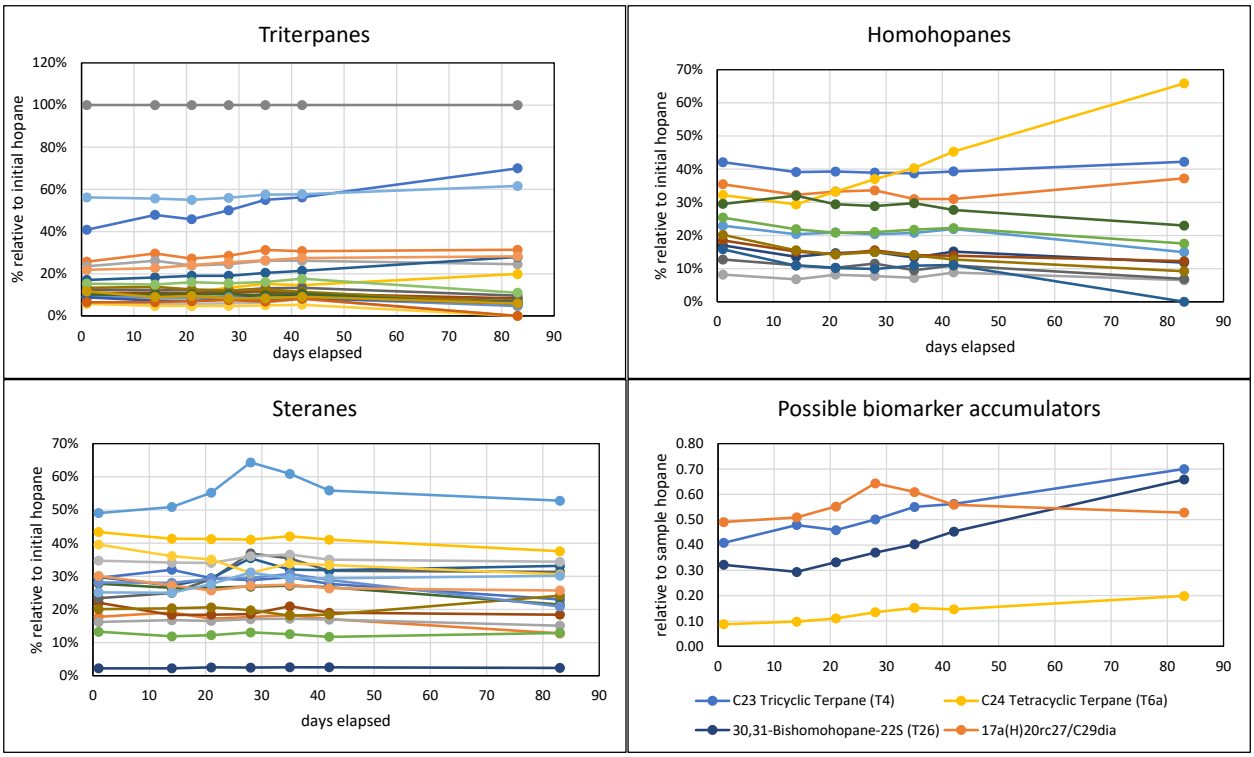

***Fig. A5-2**. Biomarker depletion relative to hopane depicts mostly simple depletion (mildly decreasing or flat trends) rather than accumulation. The few accumulating examples (lower right panel – duplicated from the three other plots) are exceptions from trace-level lab artifacts.*

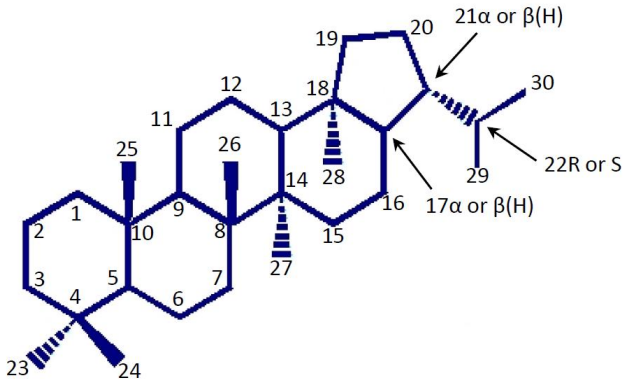

***Fig. A5-3**. Carbon model of 17α(H),21β(H)-hopane. The node of each solid line represents a carbon atom (here numbered, 1-30). Solid and dashed triangles indicate upper or downward projection of carbons. The αβ, ββ, or βα stereoisomers describe alternative hydrogen projections.*

But even if derived from lipid membranes, they seem unlikely to reincorporate or for there to be sufficient “free energy” to slip through them. Hopanes comprise three stereoisomeric series: 17α(H),21β(H)-, 17β(H), 21β(H)-, and 17β(H),21α(H)-hopanes, with the α and β notations indicating whether the hydrogen atoms are below or above the plane of the page, respectively (Fig. A5-3). Hopanes with the αβ configuration are characteristic of petroleum because of their greater thermodynamic stability, relative to the other configurations (ββ, βα), following eons of microbial, heat, and pressure maturation in the oil formation. The major precursors for the hopanes in living organisms have “biological” or ββ stereochemistry, which is almost flat but not a planar aromatic molecule like the 4 and 5-ring PAH. Those saturated six-member hopane rings can exist in either a “boat or chair” configuration as controlled by the stereochemistry and the position of alkyl and hydrogen substituents. Hopanes are also amphipathic (e.g., having both hydrophilic and lipophilic structural components), which combined with the flatter ββ configuration, appears to be necessary for insertion into lipid membranes. In oil formations, because the ββ stereochemical arrangement is thermodynamically less stable, diagenesis and catagenesis of the precursors result in transformation of ββ precursors to αβ hopane, the petroleum biomarker. Per free-energy models (Endo et al., 2011), we speculate that the αβ hopanes with their protruding methyl groups and hydrogens (Fig. A5-3) are unlikely to slip into alignment with the ββ forms in order to enter living membranes nor be efficiently processed by metabolic enzymes into storage lipids. And perhaps, this accounts for their anomalous lipophobic behavior in mussels (Fig. A5-3).

If the molecular configuration produces both hydrophobic and lipophobic behavior in tissues, then despite its high theoretical K_{LIPW}, the hopane depletion curve makes sense. It suggests biomarkers are not bioavailable to the mussel or its gut microbes. Regarding hopane’s short half-life in mussels, recent work by Staniszewska et al. (2017) corroborates that with less lipophilic hydrocarbons (bisphenol A, BPA in their study), even the portion collected by lipids in the digestive tract, can in theory be eliminated faster. Similarly, their seabird guano study (Staniszewska et al., 2014) reported smaller BPA accumulation in tissues, with a simultaneous increase in elimination compared to the removal of higher K_{OW}, alkylphenols. Work by Farrington et al. (2020) supports this concept, demonstrating longer retention as PAH increase in alkylation and molecular weight in spill contaminated mussels.

Cluster analyses

Several iterations of hierarchical agglomerative cluster analysis of the C2-normalized, times-series PAH data proved to be non-insightful. There were tendencies to form groupings affiliated with log K_{OW} values and thus to have PAH with accumulating patterns loosely group together. But there were also many outliers with disparate log K_{OW} levels placed into the various groupings. Correlations between PAH and transcription levels were also nonproductive, which may be expected considering the poor correlation of monotonically decreasing PAH levels relative to the lagged peaking-and-descending transcription values.

References

Balseiro, P.; Falcó, A.; Romero, A.; Dios, S.; Martínez-López, A.; Figueras, A.; Estepa, A.; Novoa, B. *Mytilus galloprovincialis* Myticin C: a chemotactic molecular with antiviral activity and immunoregulatory properties. *PLOS ONE* **2011**, *6*, e23140. DOI 10.1371/journal.pone.0023140.

Banni, M.; Dondero, F.; Jebali, J.; Guerbej, H.; Boussetta, H.; Viarengo, A. Assessment of heavy metal contamination using real-time PCR analysis of mussel metallothionein mt10 and mt20 expression: a validation along the Tunisian coast. *Biomarkers* **2007**, *12*, 369-383; DOI 10.1080/13547500701217061.

Banni, M.; Negri, A.; Mignone, F.; Boussetta, H.; Viarengo, A.; Dondero, F. Gene expression rhythms in the mussel *Mytilus galloprovincialis* (Lam.) across an annual cycle. *PLOS ONE* **2011**, *6*, e18904. DOI 10.1080/13547500701217061.

Blumer, M.; Mullin, M. M.; Thomas, D. W. Pristane in zooplankton. *Science* **1963**, *140*, 974.

Blumer, M.; Guillard, R. R. L.; Chase, T. Hydrocarbons of marine phytoplankton. *Mar. Biol.* **1971**, *8*, 183-189.

Bourdon, J. C. p53 and its isoforms in cancer. *Brit. J. Cancer*, **2007**, *97*, 277-282; DOI 10.1038/sj.bjc.6603886.

Bowen, L.; Miles, A. K.; Ballachey, B.; Waters, S.; Bodkin, J.; Lindeberg, M.; Esler, D. Gene transcription patterns in response to low level petroleum contaminants in *Mytilus trossulus* from field sites and harbors in southcentral Alaska. *Deep-Sea Res. Part II* **2018**, *147*, 27-35; DOI 10.1016/j.dsr2.2017.08.007.

Cellura, C.; Toubiana, M.; Roch, P. Specific expression of antimicrobial peptide and HSP70 genes in response to heat-shock and several bacterial challenges in mussels. *Fish Shellfish Immun*. **2007**, *22*, 340-350; DOI 10.1016/j.fsi.2006.06.007.

Châtel, A.; Faucet-Marquis, V.; Gourlay-Francé, C.; Pfohl-Leszkowicz, A.; Vincent-Hubert, F. 2015. Genotoxicity and activation of cellular defenses in transplanted zebra mussels *Dreissena polymorpha* along the Seine river. *Ecotox. Environ. Safe*. **2015**, *114*, 241-249; DOI 10.1016/j.ecoenv.2014.03.023.

Chen, Z. F.; Wang, H.; Matsumura, K.; Qian, P. Y. Expression of calmodulin and myosin light chain kinase during larval settlement of the barnacle *Balanus amphitrite*. *PLOS ONE* **2012**, 7, e31337. DOI 10.1371/journal.pone.0031337.

De Maio, A. M. Heat shock proteins: facts, thoughts, and dreams. *Shock* **1999**, *11*, 1-2; DOI 10.1097/00024382-199901000-00001.

Di, Y.; Schroeder, D. C.; Highfield, A.; Readman, J. W.; Jha, A. N. Tissue-specific expression of p53 and ras genes in response to the environmental genotoxicant benzo (*a*) pyrene in marine mussels. *Environ. Sci. Technol.* 2011, *45*, 8974-8981; DOI 10.1021/es201547x.

Endo, S.; Escher, B. I.; Goss, K. Capacities of membrane lipids to accumulate neutral organic chemicals. *Environ. Sci. Technol*. 2011, *45*, 5912-5921; DOI 10.1021/es200855w.

Farrington, J. W.; Davis, A. C.; Frew, N. M.; Rabin, K. S. No. 2 fuel oil compounds in *Mytilus edulis*. Retention and release after an oil spill. *Mar. Biol*. 1982, *66*, 15-26.

Farrington, J. W.; Jia, X.; Tripp, B. W.; Livramento, J. B. Fuel oil hydrocarbons in *Mytilus edulis* in Buzzards Bay, Massachusetts USA: Comparison of data from two oil spills. *Mar. Pollut. Bull*. 2020, *153*, 111034. DOI 10.1016/j.marpolbul.2020.111034.

Franzellitti, S.; Buratti, S.; Donnini, F.; Fabbri, E. Exposure of mussels to a polluted environment: Insights into the stress syndrome development. *Comp. Biochem. Phys. C*. 2010, *152*, 24-33; DOI 10.1016/j.cbpc.2010.02.010.

Fukuda, R.; Zhang, H.; Kim, J. W.; Shimoda, L.; Dang, C. V.; Semenza, G. L. HIF-1 regulates cytochrome oxidase subunits to optimize efficiency of respiration in hypoxic cells. *Cell* 2007, *129*, 111-122; DOI 10.1016/j.cell.2007.01.047.

Giannetto, A.; Maisano, M.; Cappello, T.; Oliva, S.; Parrino, V.; Natalotto, A.; De Marco, G.; Barberi, C.; Romeo, O.; Mauceri, A.; Fasulo, S. Hypoxia-inducible factor *α* and Hif-prolyl hydroxylase characterization and gene expression in short-time air-exposed *Mytilus galloprovincialis*. *Mar. Biotechnol.* 2015, *17*, 768-781; DOI 10.1007/s10126-015-9655-7.

Giuliani, M. E.; Benedetti, M.; Arukwe, A.; Regoli, F. Transcriptional and catalytic responses of antioxidant and biotransformation pathways in mussels, *Mytilus galloprovincialis*, exposed to chemical mixtures. *Aquat. Toxicol.* 2013, 120-127; DOI 10.1016/j.aquatox.2013.03.012.

Goodson, M. S.; Crookes-Goodson, W. J.; Kimbell, J. R.; McFall-Ngai, M. J. Characterization and role of p53 family members in the symbiont-induced morphogenesis of the *Euprymna scolopes* light organ. *Biol. Bull.* 2006, *211*, 7-17; DOI 10.2307/4134573.

Hüning, A. K.; Melzner, F.; Thomsen, J.; Gutowska, M. A.; Kramer, L.; Frickenhaus, S.; Rosenstiel, P.; Pörtner, H. O.; Philipp, E. E. R.; Lucassen, M. Impacts of seawater acidification on mantle gene expression patterns of the Baltic Sea blue mussel: implications for shell formation and energy metabolism. *Mar. Biol.* 2013, *160*, 1845-1861; DOI 10.1007/s00227-012-1930-9.

Iwama, G. K.; Mathilakath, M. V.; Forsyth, R. B.; Ackerman, P. A. Heat shock proteins and physiological stress in fish. *Am. Zool.* 1999, *39*, 901-909; DOI 10.1093/icb/39.6.901.

Lacroix, C.; Coquillé, V.; Guyomarch, J.; Auffret, M.; Moraga, D. A selection of reference genes and early-warning mRNA biomarkers for environmental monitoring using *Mytilus* spp. as sentinel species. *Mar. Pollut. Bull.* **2014**, *86*, 304-313; DOI 10.1016/j.marpolbul.2014.06.049.

Li, S.; Xie, L.; Zhang, C.; Zhang, Y.; Gu, M.; Zhang, R. Cloning and expression of a pivotal calcium metabolism regulator: calmodulin involved in shell formation from pearl oyster (*Pinctada fucata*). *Comp. Biochem. Phys. A.* **2004**, *138*, 235-243; DOI 10.1016/j.cbpc.2004.03.012.

Livak, K. J.; Schmittgen, T. D. Analysis of relative gene expression data using real-time quantitative PCR and the 2− ΔΔCT method. *Methods*, **2001**, *25*, 402-408; DOI 10.1006/meth.2001.1262.

Mason, R. P. Accumulation and depuration of petroleum hydrocarbons by black mussels. 1. Laboratory exposure trials. *S. Afr. J. Marine Sci*. **1988**, *6*, 143-153; DOI 10.2989/025776188784480582.

Mitta, G.; Hubert, F.; Dyrynda, E. A.; Boudry, P.; Roch, P. Mytilin B and MGD2, two antimicrobial peptides of marine mussels: gene structure and expression analysis. *Dev. Comp. Immunol.* **2000**, *24*, 381-393; DOI 10.1016/S0145-305X(99)00084-1.

Murray, I. A.; Patterson, A. D.; Perdew, G. H. Aryl hydrocarbon receptor ligands in cancer: friend and foe. *Nat. Rev. Cancer*, **2014**, *14*, 801-814; DOI 10.1038/nrc3846.

National Research Council (NRC). Oil in the Sea; Inputs, Fates and Effects. National Academy Press, Washington, D.C., **1985**.

Payne, J. R.; Driskell, W. B.; Short, J. W.; Larsen, M. L. *Exxon Valdez Oil Spill Restoration Project Final Report: 2004-2005 LTEMP Oil Monitoring Report*; Restoration Project No. 040724; PWSRCAC Contract No. 951.05.1: Alaska, **2006**;

Place, S. P.; O'Donnell, M. J.; Hofmann, G. E. Gene expression in the intertidal mussel *Mytilus californianus*: physiological response to environmental factors on a biogeographic scale. *Mar. Ecol. Prog. Ser.*, **2008**, *356*, 1-14; DOI 10.3354/meps07354.

Romero, A.; Estévez-Calvar, N.; Dios, S.; Figueras, A.; Novoa, B. New insights into the apoptotic process in mollusks: characterization of caspase genes in *Mytilus galloprovincialis*. *PLOS ONE* **2011**, *6*, e17003. DOI 10.1371/journal.pone.0017003.

Staniszewska, M.; Falkowska, L.; Grabowski, P.; Kwasniak, J.; Mudrak-Cegiołka, S.; Reindl, A. R.; Sokołowski, A.; Szumiło, E.; Zgrundo, A. Bisphenol A, 4-tertoctylphenol, 4- nonylphenol in the gulf of Gdansk (southern Baltic). *Arch. Environ. Con. Tox.* **2014**, *67*, 335e347. DOI 10.1007/s00244-014-0023-9.

Staniszewska, M.; Graca, B.; Sokołowski, A.; Nehring, I.; Wasik, A.; Jendzul, A. Factors determining accumulation of bisphenol A and alkylphenols at a low trophic level as exemplified by mussels *Mytilus trossulus. Environ. Pollut*. **2017**, *220*, 1147-1159; DOI 10.1016/j.envpol.2016.11.020.

Stegeman, J. J.; Teal, J. M. Accumulation, release and retention of petroleum hydrocarbons by the oyster *Crassostrea virginica*. *Mar. Biol.* **1973**, *22*, 37-44. DOI 10.1007/BF00388908.

Sureda, A.; Box, A.; Tejada, S.; Blanco, A.; Caixach, J.; Deudero, S. Biochemical responses of *Mytilus galloprovincialis* as biomarkers of acute environmental pollution caused by the Don Pedro oil spill (Eivissa Island, Spain). *Aquat. Toxicol.* **2011**, *101*, 540-549; DOI 10.1016/j.aquatox.2010.12.011.

Tsan, M.; Gao, B. Cytokine function of heat shock proteins. *Am. J. Physiol.-Cell Ph*. **2004**, *286*, C739-C744; DOI 10.1152/ajpcell.00364.2003.

Woo, S.; Jeon, H. Y.; Kim, S. R.; Yum, S. Differentially displayed genes with oxygen depletion stress and transcriptional responses in the marine mussel, *Mytilus galloprovincialis*. *Comp. Biochem. Phys. D* **2011**, *6*, 348-356; DOI 10.1016/j.cbd.2011.07.003.

Woo, S.; Denis, V.; Won, H.; Shin, K.; Lee, G.; Lee, T. K.; Yum, S. Expressions of oxidative stress-related genes and antioxidant enzyme activities in *Mytilus galloprovincialis* (Bivalvia, Mollusca) exposed to hypoxia. *Zool. Stud.* **2013**, *52*, 15; DOI 10.1186/1810-522X-52-15.

Wu, R. Hypoxia: from molecular responses to ecosystem responses. *Mar. Pollut. Bull.* **2002**, *45*, 35-45; DOI 10.1016/S0025-326X(02)00061-9.

Xie, F.; Xiao, P.; Chen, D.; Xu, L.; Zhang, B. miRDeepFinder: a miRNA analysis tool for deep sequencing of plant small RNAs. *Plant Mol. Biol.* **2012**, *80,* 75-84; DOI 10.1007/s11103-012-9885-2.

Zanette, J.; Jenny, M. J.; Goldstone, J. V.; Parente, T. Woodin, B. R.; Bainy, A. C.; Stegeman, J. J. Identification and expression of multiple CYP1-like and CYP3-like genes in the bivalve mollusk *Mytilus edulis*. *Aquat. Toxicol.* **2013**, *128*, 101-112; DOI 10.1016/j.aquatox.2012.11.017.

Zeng, L. G.; Wang, J. H.; Li, Y. J.; Sheng, J. Q.; Gu, Q.; Hong, Y. J. Molecular characteristics and expression of calmodulin cDNA from the freshwater pearl mussel, *Hyriopsis schlegelii*. *Genet. Mol. Res.* **2012**, *11*, 42-52; DOI 10.4238/2012.January.9.5.